

Journal of Visualized Experiments

Preparing lamellae from vitreous biological samples using a dual-beam scanning electron microscope for cryo-electron tomography --Manuscript Draft--

| | |
|--|---|
| Article Type: | Invited Methods Collection - JoVE Produced Video |
| Manuscript Number: | JoVE62350R1 |
| Full Title: | Preparing lamellae from vitreous biological samples using a dual-beam scanning electron microscope for cryo-electron tomography |
| Corresponding Author: | Claudine Bisson King's College London London, London UNITED KINGDOM |
| Corresponding Author's Institution: | King's College London |
| Corresponding Author E-Mail: | claudine.bisson@kcl.ac.uk |
| Order of Authors: | Claudine Bisson Corey W. Hecksel James B. Gilchrist Roland Fleck |
| Additional Information: | |
| Question | Response |
| Please indicate whether this article will be Standard Access or Open Access. | Open Access (US\$4,200) |
| Please specify the section of the submitted manuscript. | Biochemistry |
| Please indicate the city, state/province, and country where this article will be filmed . Please do not use abbreviations. | London, UK |
| Please confirm that you have read and agree to the terms and conditions of the author license agreement that applies below: | I agree to the Author License Agreement |
| Please provide any comments to the journal here. | |
| Please indicate whether this article will be Standard Access or Open Access. | Open Access (\$3900) |

TITLE:

Preparing Lamellae from Vitreous Biological Samples using a Dual-Beam Scanning Electron Microscope for Cryo-Electron Tomography

AUTHORS AND AFFILIATIONS:

Claudine Bisson^{1,2*}, Corey W. Hecksel^{3,4}, James B. Gilchrist³, Roland Fleck^{1*}

¹Centre for Ultrastructural Imaging, New Hunt's House, Guy's Campus, King's College London, London, UK.

²Department of Biological Science, Birkbeck College, University of London, Malet Street, London, UK.

³Electron Bio-Imaging Centre, Diamond Light Source, Harwell Science and Innovation Campus, Didcot, UK.

⁴Current address: SLAC National Accelerator Laboratory, Stanford University, 2575 Sand Hill Rd, Menlo Park, California

E-mail addresses of authors:

Claudine Bisson (claudine.bisson@kcl.ac.uk)

Corey W. Hecksel (hecksel@stanford.edu)

James B. Gilchrist (james.gilchrist@diamond.ac.uk)

Roland Fleck (roland.fleck@kcl.ac.uk)

***Corresponding authors:**

Roland Fleck (roland.fleck@kcl.ac.uk)

Claudine Bisson (claudine.bisson@kcl.ac.uk)

KEYWORDS:

FIB-milling, cryoFIB-SEM, lamella, tomography, cryoET, cryoEM, *Plasmodium falciparum*

SUMMARY:

Using focused ion beam milling to produce vitreous on-grid lamellae from plunge frozen biological samples for cryo-electron tomography.

ABSTRACT:

Presented here is a protocol for preparing cryo-lamellae from plunge-frozen grids of *Plasmodium falciparum*-infected human erythrocytes, which could easily be adapted for other biological samples. The basic principles for preparing samples, milling, and viewing lamellae are common to all instruments and the protocol can be followed as a general guide to on-grid cryo-lamella preparation for cryo-electron microscopy (cryoEM) and cryo-electron tomography (cryoET). Electron microscopy grids supporting the cells are plunge-frozen into liquid nitrogen-cooled liquid ethane using a manual or automated plunge freezer, then screened on a light microscope equipped with a cryo-stage. Frozen grids are transferred into a cryo-scanning electron microscope equipped with a focused ion beam (cryoFIB-SEM). Grids are routinely sputter coated prior to milling, which aids dispersal of charge build-up during milling.

Alternatively, an e-beam rotary coater can be used to apply a layer of carbon-platinum to the grids, the exact thickness of which can be more precisely controlled. Once inside the cryoFIB-SEM an additional coating of an organoplatinum compound is applied to the surface of the grid via a gas injection system (GIS). This layer protects the front edge of the lamella as it is milled, the integrity of which is critical for achieving uniformly thin lamellae. Regions of interest are identified via SEM and milling is carried out in a step-wise fashion, reducing the current of the ion beam as the lamella reaches electron transparency, in order to avoid excessive heat generation. A grid with multiple lamellae is then transferred to a transmission electron microscope (TEM) under cryogenic conditions for tilt-series acquisition. A robust and contamination-free workflow for lamella preparation is an essential step for downstream techniques, including cellular cryoEM, cryoET, and sub-tomogram averaging. Development of these techniques, especially for lift-out and milling of high-pressure frozen samples, is of high-priority in the field.

INTRODUCTION:

Only the cellular contents of biological samples <500 nm thick can be imaged effectively by transmission electron microscopy (TEM) at cryogenic temperatures, limiting the range of specimens to viruses, prokaryotes, simple single-cellular organisms, and thinner regions of larger eukaryotic cells¹. On-grid focused ion beam (FIB)-milling enables thicker plunge-frozen biological samples to be thinned to form electron transparent lamellae at cryogenic temperatures (< -150 °C). The resulting lamellae are then transferred to a TEM for visualization and tomographic data collection, enabling high-resolution 3D reconstructions of the cellular and molecular features inside of cells (for reviews see Rigort et al., 2012², Oikonomou et al., 2016³, and Wagner et al., 2020⁴).

FIB-milling emerged from the field of materials sciences, where samples are routinely thinned to prepare them for downstream analysis⁵. It is carried out in a scanning electron microscope (SEM), which has two optical columns: conventional scanning electron microscope optics and a second column containing optics able to generate and finely control a focused ion beam (FIB) – called a FIB-SEM. This allows a specific region of the sample to be ablated by ions generated by a gallium source, removing excess material and leaving behind a lamella⁶. The milling process is guided by SEM imaging of the topography of the sample, which is used to locate regions of interest and monitor milling progress. For biological applications, the basic setup is largely the same, but milling is carried out at cryogenic temperatures. This has required standard FIB-SEMs to be adapted to have cryo-cooled stages that maintain constant temperatures and low surface contamination rates, as well as airlocks to facilitate sample transfer without devitrification or contamination. Sample shuttles have also been modified to permit a range of different carriers to be mounted inside the cryoFIB-SEM, including TEM grids, planchettes, and capillaries. Several key groups of researchers have been central to the development of these methods and the continuing technological advances in this area^{7–12}. Commercial solutions are now more widely available for biological FIB-milling at cryogenic temperature and on-grid milling of lamellae is becoming more routine, given an optimized sample.

A range of room temperature and cryoEM techniques can be used to visualize cellular

information across all scales of life, from whole multicellular organisms at modest resolution to understanding the context of complex processes at the cellular level and in even greater detail, to the determination of *in situ* molecular structures^{13–19}. Classical room temperature techniques include sectioning fixed and stained, resin imbedded cells and tissues by ultramicrotomy for analysis of cellular morphology by TEM (for review see Studer et al., 2008²⁰). Alternative techniques have been developed exploiting secondary electron scattering by SEM to image the surface of blocks of preserved cells, before progressively removing material either with a knife (serial block face imaging) or a focused ion beam^{21–23}. This technique has also been successfully implemented at cryogenic temperatures (referred to as cryo-volume imaging) with a cryoFIB-SEM on vitreous, unstained blocks of cells or tissues²⁴. Alternatively, thicker lamellae (~15 µm thick) can be milled and studied by STEM imaging²⁵. Using these techniques, whole blocks containing many cells can be imaged to gather population information or a whole organ/organism can be imaged and reconstructed in 3D. However, to access high-resolution molecular information from cells, samples need to be preserved in a near-native, frozen-hydrated state and, therefore, need to be prepared under cryogenic conditions. Cryo-electron microscopy of vitreous sections (CEMOVIS) is a technique whereby high-pressure frozen blocks of biological material are sectioned under cryogenic conditions with an ultramicrotome. This produces ribbons cryo-sections (40–100 nm thick)²⁶, which are attached to an EM grid and imaged in the TEM. However, the physical interaction of the knife with the vitreous sample causes crevassing and compression artifacts that can severely distort cellular structure^{27–30}. Thicker sections are more prone to these artefacts, making it impractical to use sections thicker than ~70 nm²⁶. This limitation greatly restricts the 3D view of the biological structure in the tomogram. FIB-milling at cryogenic temperatures does not experience these problems, but has its own artifacts caused by differential milling rates across parts of the specimen, leading to variable thicknesses within a lamella – called curtaining. This problem is mitigated by the application of an organoplatinum coat applied via a gas injection system (GIS), which protects the front edge of the lamella during milling³¹. The upper limit of sample thickness for on-grid FIB-milling is defined by the ability to plunge freeze the specimen while keeping it vitreous³², although, with the introduction of cryo lift-out techniques and adapted sample carriers for biological specimens, FIB-milling can also be used to process high-pressure frozen samples^{31,33–35}. Additionally, plunge frozen samples cannot be too thin as there must be enough biological material to generate a reasonably sized lamella that will provide enough surface area to collect tilt-series at the required magnification. This, however, can be mitigated by milling clumps of smaller cells, such as bacteria or yeast. Final lamella thickness (~100–300 nm) is usually dictated by the sample integrity and milling strategy. Thinner lamellae are better for high-resolution structural work, such as sub-tomogram averaging, but thicker lamellae contain much larger cellular volumes than can be achieved by CEMOVIS, providing more cellular context in a near to natively preserved sample. FIB-milling can also be used to thin plunge-frozen protein crystals for electron diffraction studies³⁶.

FIB-milling of vitreous cells is worth the time and effort to carry out if the scientific question requires high-resolution molecular detail of near-native specimens *in situ*. With access to more facilities for the routine production of lamellae, the rate limiting step is often the optimization of the sample prior to milling, where time must be taken to ensure the sample is vitreous and

an appropriate thickness to produce robust and uniformly thin lamellae. Described here is the sample optimization for FIB-milling plunge-frozen human red blood cells infected with the *Plasmodium falciparum* parasites, the causative agent of malaria, but this approach could be adapted for any given sample.

PROTOCOL:

Human blood was obtained from anonymized donors through the UK National Blood and Transplant service and is used within 2 weeks of receipt. No ethical approval is required for its use.

1. Preparation and plunge freezing of *Plasmodium falciparum* infected red blood cells

1.1. Isolate mature schizonts by centrifugation (1,580 x *g*) over a 70% (v/v) isotonic density gradient medium (for standard procedures for how to culture asexual blood stages of 3D7 *Plasmodium falciparum* in human erythrocytes see Blackman M.J., 1995³⁷).

1.2. Fix the air-dried thin blood films on a glass slide with 100% methanol to check the morphological homogeneity of the schizonts before staining with 10% Giemsa stain in 6.7 mM phosphate buffer, pH 7.1.

NOTE: To enrich the preparation for schizonts stalled at specific points of egress, schizonts can be further synchronized with compound 2 and E64 inhibitors (see **Representative Results** and **Figure 1** for an explanation of the effect of these inhibitors).

CAUTION: *Plasmodium falciparum* is a human pathogen and must only be handled in a suitable containment facility following local health and safety guidelines.

1.3. Gently centrifuge schizonts (240 x *g*) to pellet them and resuspend in 2x volume of the cell pellet of RPMI media, resulting in a 50% haematocrit suspension.

1.4. On a manual plunge freezing rig, apply 2.5 µL of schizonts to the carbon side of a glow-discharged (60 s, 30 mA in air, on the carbon side only using a glow discharge unit) 200 mesh copper grid with a 2/4 holey carbon film and blot for ~20 s from the back of the grid using grade 1 filter paper with a torn edge. Plunge into liquid nitrogen-cooled liquid ethane and transfer the grids to storage.

NOTE: The experiment can be paused here, and grids can be stored under liquid nitrogen indefinitely.

CAUTION: Liquid nitrogen is an asphyxiant and causes frostbite; handle with care in a suitable environment with oxygen monitoring.

CAUTION: Liquid ethane causes severe burns and is flammable; use in a fume hood away from

sources of ignition.

NOTE: Plunge frozen schizonts are no longer viable. This was determined by incubating human blood with several gold grids of air-thawed plunge-frozen schizonts and observing no parasite growth after several days, in comparison to un-frozen controls. Frozen grids of schizonts are therefore safe to handle outside of containment facilities using normal safety and decontamination procedures (gloves, surface/tool sterilization with >70% ethanol and disposal of grids in >70% ethanol).

1.5. Screen grids using a cryo-stage for a light microscope (see **Table of Materials** for equipment used in this study), paying particular attention to the gradient of ice across the grid. In the thinner areas of ice, check individual grid squares for cell coverage.

NOTE: The best squares should be one cell thick at the center of the grid square (**Figure 2**). This ensures that a lamella can be milled across the center of the square without hitting the thicker ice at the edges against the grid bars. The experiment can be paused here, and grids can be stored under liquid nitrogen indefinitely. If cells carry a fluorescent marker, grids can also be screened by cryoCLEM to locate X/Y positions of interest, which can be correlated with grid locations in the cryoFIB-SEM to direct milling.

2. On-grid FIB-milling of plunge frozen cells

2.1. Mark the front of cryoFIB-specific autogrid rims with a black indelible marker pen to indicate the center of the cutaway section and the opposite side of the rim (**Figure 3**). Setup the clipping station and clip grids into the marked rings carbon side down.

2.2. Load grids into the cryoFIB-SEM shuttle (typically 2 grids, depending on the shuttle) carbon side up and apply a platinum sputter coat in an argon atmosphere (5×10^{-2} mbar) (5 mA for 60 s – thickness is variable) or a carbon/platinum e-beam rotary coat (~4 nm thickness) to the surface of the cells.

NOTE: Both types of coatings aid charge dispersal during SEM imaging. The benefit of the e-beam rotary coater is that the exact thickness of the coating can be specified.

2.3. Load the shuttle into the cryoFIB-SEM and assess the cell distribution on each grid by SEM at 5 kV (13 pA or 25 pA). Take a low-magnification overview (~100x) to look at ice gradients across the grid. Then, take higher-magnification (~5,000x) images to look at individual grid squares and identify the areas of the grid with visible cellular features and low surface contamination to mill.

2.4. Apply a >2 μm organoplatinum coat to the surface of each grid using the gas injection system (GIS). To do this, insert the GIS needle into the chamber above the grid and warm the organoplatinum source to a set temperature for a set time (for example, ~27 °C for 3–10 s) to produce a flow of vapor.

NOTE: The angle of application, temperature, and timing of the organoplatinum coat via the GIS needle should be optimized to maximize an even coating. This will depend on the specific cryoFIB-SEM used (see **Representative Results** for further explanation).

2.5. Tilt the sample so that the plane of the grid is $\sim 10^\circ$ from the incidence angle of the ion beam and move the center of a suitable grid square to be seen in both the SEM and FIB images.

2.6. Survey the grid using the ion beam at low current (nominally 1.5 pA, 30 kV) and go to high enough magnification ($\sim 7,000\times$) to visualize the cells at the center of a grid square. Bring the sample into focus at the first milling current (300 pA) and correct for astigmatism. Adjust the brightness and the contrast, then mark out two rectangular patterns to mill, one above and one below a 3 μm thick protected region, the center of which is the desired location of the final lamella.

NOTE: The chosen width of the patterns will depend on the topography of the surrounding cell layer and the cell size. 7–20 μm work well for schizonts, but wider lamellae take longer to mill. The chosen height of the patterns for the first milling step depends on the sample thickness, starting around 6 μm ; this may need to be adjusted during milling. Milling is carried out directionally from the outside top and bottom edges of the patterns toward the face of the lamella. This can be done in parallel, where both patterns are milled concurrently or sequentially, first removing material from above the lamella and then from underneath.

2.7. Start milling at the first current; monitor the live progress in the ion beam view and intermittently by SEM (5 kV, 13 or 25 pA). Check that the ion beam has broken through the sample above and below the protected region. If not, increase the height of the rectangular patterns to remove more material. Stop when the surface above and below the lamella is completely smooth in the ion beam view.

NOTE: The ion beam has broken through the sample above and below the protected region when the inside of the rectangular patterns contains no features in the focal plane. Some features, such as grid bars, may be visible out of focus in the background.

2.8. Change to the next milling current (100 pA); focus and adjust the brightness/contrast. Decrease the space between the two rectangular patterns to 1.5 μm and decrease the pattern height to only cover the un-milled material. Begin milling at the new current until the surface above and below the lamella is completely smooth.

2.9. Repeat this process stepwise until a thickness of 0.3 μm is reached, reducing the ion beam current each time according to the milling scheme in **Table 1**.

2.10. Mill several lamellae (the amount is dependent on the thickness of the sample and the time available) on one or both grids to a thickness of 0.3 μm , record the X/Y/Z position of each lamella and reserve $\sim 1\text{--}2$ h at the end of the session to polish the lamellae to their final

thickness (60–200 nm).

2.11. Take a low-magnification SEM overview of the entire grid and plan a polishing route starting from lamellae at the front of the grid (closer to the ion beam source) to lamellae at the back of the grid (furthest away from the ion beam source) (**Figure 5**).

NOTE: This reduces redeposition of ablated material back onto the surface of polished lamellae.

2.12. Reduce the space between the two rectangular patterns to 100–200 nm and begin the final polishing step at an ion beam current of 30 pA. Monitor the progress by SEM at 2–3 kV (13 pA, dwell = 300 n, 3072 x 2048, ~2 s for a full frame) and stop polishing when the contrast is lost in the lamella by SEM and when the organoplatinum coat or the lamella itself begins to lose integrity.

2.13. Before removing the grids, acquire a low-magnification SEM image of the entire grid and save images of each lamella. Use them to cross-check the grid later in the TEM. Pause the experiment here and store the grids with lamellae under liquid nitrogen – handle with care.

NOTE: Grids can be lightly sputter coated upon removal from the cryoFIB-SEM, which can help limit drift and charging in the TEM at high-magnification, but this should be done cautiously as too much sputter coating can obscure the biological contents inside the lamellae. It is possible to screen lamellae for fluorescence at this stage; however, obtaining enough signal will depend on the abundance of the labeled protein within the thickness of the lamella. Great care must be taken handling the grids to limit damage to the lamellae and prevent surface contamination.

3. Tilt-series acquisition and general overview of data processing

3.1. Load the grids into the TEM, aligning the milling direction perpendicular to the tilt axis of the stage.

NOTE: Alignment of the grids is done by eye using the marks on the autogrid rim. A ~10° margin of error is acceptable, otherwise the walls of the trench either side of the lamella may obscure the lamella as the grid is tilted.

3.2. Acquire a low-magnification map (~150x) of the entire grid and locate the lamellae; then, acquire a medium-magnification map (~1,500x, depending on lamella size) of each lamella and locate the areas of interest.

3.3. Pre-tilt the grid by $\pm 10^\circ$ to make the plane of the lamella (not the grid) perpendicular to the optical axis.

NOTE: The direction of the pre-tilt can be determined by the position of the front edge of the lamellae (looking for the left over organoplatinum coat) in the map. For the TEM used here, it required a +10° pre-tilt if the front edges of the lamellae pointed up in the montage and

required a -10° pre-tilt if they pointed down. Each grid may be different due to how they were picked up and inserted into the autoloader.

3.4. Acquire dose-symmetric tilt-series³⁸ (for example, -54° to $+54^\circ$ with an increment of $3-5^\circ$) at a pixel size that permits both the field of view and resolution required for the region of interest. Use a range of defocus values between -2 and $-5\ \mu\text{m}$. Collect movies with $3-10$ frames at each increment and for this, adjust these parameters depending on the pixel size to accumulate a total dose of $\sim 150\ \text{e}^-/\text{\AA}^2$ (for a $300\ \text{kV}$ TEM).

NOTE: Cracks in the lamella should be avoided as these regions may drift. Surface contamination should also be avoided as it may obscure the region of interest or the focus area at high-tilt.

3.5. Motion correct the movies using a program such as MotionCor2³⁹. Apply a dose weighting filter to the corrected images (accumulated e^-/image)⁴⁰ and estimate the defocus of each image using a program such as CTFFIND4⁴¹.

3.6. Use fiducial-less alignment (patch tracking) in a program such as etomo (IMOD)⁴² to calculate the alignment and angular relationship of the images in tilt-series.

3.7. Input the alignment and rotation information, along with the defocus values into a program that can apply three dimensional CTF correction, for example, NovaCTF⁴³. Calculate a corrected tomogram to get output tomograms with binning factors relevant to downstream analysis.

3.8. Analyze the reconstructions and prepare for any downstream processing, for example, filtering, segmentation, or sub-tomogram averaging.

REPRESENTATIVE RESULTS:

Preparing *P. falciparum* schizonts for plunge freezing

Compound 2 and E64 inhibitors are used to stall schizonts at different stages of egress, generating an enriched population of schizonts for subsequent study. This is important because without a complementary correlative technique, milling specific sub-cellular targets or cell-types is challenging as the process is essentially blind. Compound 2 is a protein kinase inhibitor that stalls egress prior to vacuole rupture. Schizonts can be synchronized on compound 2 for $4\ \text{h}$, then washed with compound 2-free media to remove the inhibitor, at which point schizonts will mature and egress after approximately $30\ \text{min}$. Alternatively, compound 2 synchronized schizonts can be washed into E64, an irreversible broad-spectrum cysteine protease inhibitor, and incubated for approximately $1\ \text{h}$ to stall egress after the point of vacuole rupture, but before host cell rupture. The morphology and homogeneity of treated schizonts should be checked by Giemsa-stained blood smears prior to plunge freezing (**Figure 1**). Schizonts can be plunge frozen in either of these states using the method described in this publication.

[Insert **FIGURE 1** here]

Optimization of plunge freezing

A range of grids with different hole sizes were trialed during the optimization of blotting conditions for *P. falciparum* infected red blood cells, including 2/2, 3/3, 3.5/1, and 5/2 (square) holey carbon on gold and copper 200 mesh grids. 200 mesh copper finder grids with 2/4 holey carbon film provide a suitably thick layer of cells to mill long vitreous lamellae. Bigger or smaller holes generally resulted in cell layers that were too thin or thick, respectively (**Figure 2A–C**). With 2/4 holey carbon, schizonts are pulled through the 2 μ m holes by blotting the grid from the back (non-carbon side), resulting in cells poking out above and below the carbon film. The 4 μ m stretch of carbon between the holes results in a strip of carbon running through the middle of most of the resulting lamellae, adding strength. Finder grids are most suitable for correlative and screening purposes⁴⁴, but care must be taken to make sure the numbers/letters in the mesh design are not too big as this will block areas for milling.

The blotting time on a manual plunger is approximately 20 s, but the exact point at which to stop blotting was judged by eye when the droplet of liquid being drawn from the grid stopped spreading out on the filter paper. A torn edge was required to break the surface tension of the drop to start the blotting process. Automated plunge freezer was not used in this study, but a reasonable starting point for this sample would be to use the same volume of cells and grid type, making sure to blot the grids from the back in conditions with high humidity (~70%) and ambient temperature (~25 °C). The blotting times and conditions would need to be optimized for the particular automated system used.

Plunge frozen grids of *P. falciparum* schizonts were screened by a light microscope equipped with a cryo-stage rather than by TEM, because the sample was not transmissible to electrons. For thinner samples, grids can be screened by TEM (whole grid atlas at ~150x magnification) prior to sample transfer into the cryoFIB-SEM, which may be a pre-requisite for accessing a national facility. Special attention should be paid to the gradient of ice thickness across the grid and also within individual grid squares. Good grid squares should be one cell thick or hit the carbon film at their center (**Figure 2C**). This avoids milling in the thicker ice against the grid bars around the edge of the grid square and will ensure the ion beam breaks through above and below the cell layer, producing a free lamella rather than a wedge. Once reproducible blotting and plunge freezing conditions have been optimized, screening is usually no longer necessary prior to FIB-milling.

[Insert **FIGURE 2** here]

Marking cryoFIB-specific autogrid rims for tomography

Typically, grids are clipped into autogrid rims prior to milling in order to ease handling and provide rigidity, which protects the lamellae from damage during the subsequent transfer steps. CryoFIB-specific autogrid rims have been engineered with a cutaway feature to help access more of the grid face during milling. It is important to orientate the milling direction perpendicular to the tilt-axis of the TEM so that tilt-series acquisition proceeds by rotating the

lamella along its length. This ensures that the high walls of the trench surrounding the lamella do not obscure the biological information as the grid is tilted.

Typically, the autogrid rim is marked to help with visual alignment within the cryoFIB-SEM shuttle and later when loading the TEM. For these samples, two marks were applied at 12 o'clock and 6 o'clock with an indelible marker (see **Table of Materials**), one within the center of the cutaway section of the clip ring and the second directly opposite (**Figure 2D**). When loading into the TEM (see **Table of Materials**), both marks should be visible either side of the loading tweezers and aligned 90° to the edge of the tweezers (**Figure 2E**). It should be noted that the manufacturer recommends aligning grids using the engraved dots on the autogrid rims, as certain inks in proximity to the ion beam can interfere with milling.

Clipped grids can be screened by light microscopy with a modified cassette for a cryo-stage, which can be beneficial to check that the clipping process has not destroyed the carbon film of the grid. Depending on the sample cassette, unclipped grids can also be milled, but great care must be taken during transfer from the cryoFIB-SEM to the TEM to limit any bending of the grid as this will break the lamellae. Unclipped grids can be loaded into the TEM by side-entry cryo-holders, but there is a high chance that the lamellae will get broken if clipping is carried out after milling.

Organoplatinum coating

Organoplatinum coating is carried out on one or both grids once they have been loaded into the cryoFIB-SEM. The needle of the gas injection system (GIS) is inserted into the chamber above the sample to direct a flow of organoplatinum vapor across the surface of the grid from a heated source for a set time. The vapor condenses on cold surfaces and forms a solid layer (~2 µm thick). The integrity of this coat is critical to enable uniformly thin lamellae to be milled. The optimal application conditions for the organoplatinum coat are usually pre-determined by the manufacturer of the instrument, but some optimization may still be required. Most systems either align the GIS needle close to the milling direction or perpendicular to the milling direction, depending on the geometry of ports on the chamber and rotational limits of the stage. Different settings can be trialed by coating the grid, milling a small region, tilting the stage, and measuring the thickness of the coat by SEM.

As well as the setup of the cryoFIB-SEM itself, a number of other factors can affect the application of the organoplatinum coat including 1) the topography of the sample, 2) surface contamination on the grid and 3) the reproducibility of the vapor flow from the GIS needle. As the GIS flow is directional, uneven topography can cause regions in the shadow of cells or surface contamination to be uncoated or have a thinner coat. This can lead to a collapse of the organoplatinum layer during polishing (**Figure 3**). When selecting an area to mill, it is necessary to be mindful of the surrounding topography, for example, large surface contamination, clumps of cells or broken carbon that project out from the surface of the grid as far as a couple of grid squares away, may block the vapor flow, creating a shadow of thinner organoplatinum that will add weakness to a lamella. Additionally, very small particles of surface contamination near to the front edge of the lamella should also be avoided as they can pop-off during milling, leaving

a weakened patch of bare ice that may result in a hole developing in the lamella. Finally, if the milling has started and the organoplatinum coat looks unstable, coat again, for longer, or swap onto a back-up grid.

[Insert **FIGURE 3** here]

Assessing grid quality in the cryoFIB-SEM and the process of milling

Once grids have been transferred to the cryoFIB-SEM the integrity of the carbon film and distribution of the cells on the grids can be screened by SEM (**Figure 4A–C**). Ice gradients, the positions of grid bars and location of grid numbers on finder grids can be checked by low-magnification SEM at 30 kV (**Figure 4B**), but the voltage should be reduced back to 5 kV while locating milling positions at high-magnification and monitoring the milling process to increase the contrast from the surface topography.

[Insert **FIGURE 4** here]

A region to be milled is selected by laying out a pair of rectangular patterns either side of a protected region at high-magnification ($\sim 7,000\times$ for schizonts) in the ion beam view (**Figure 4D**). It is critical that no particles of surface contamination are attached near to the milling region as these may have obscured the application of the protective organoplatinum coat. It is also important that the topography of the region is suitable to support the sides of the lamella once its final thickness has been achieved.

For malarial schizonts (cell size: $\sim 5\ \mu\text{m}$ diameter $\times 2\ \mu\text{m}$ thick, disc-shape) lamellae between 7–20 μm wide can be milled. If the cell layer is suitably thick, the lamellae will usually end up ~ 10 –15 μm in length, capturing multiple cells above and below the carbon layer (**Figure 4E–F**). It can be expected to mill 5–10 lamellae in an 8 h session (6–7 h of milling and 1–2 h of polishing). This will vary depending on the thickness of the sample and width of the lamellae, with thicker samples and wider lamellae taking longer to mill. Even damaged grids can be milled as it requires only a handful of good grid squares to generate a set of lamellae (**Figure 5A**). Additionally, if the sample is thinner than expected, for example, due to over-blotting or variation in the haematocrit of the culture, shorter lamellae can be milled relatively quickly; however, their shorter length will limit the area available for data collection in the TEM (**Figure 5B**).

[Insert **FIGURE 5** here]

During polishing, the final thickness of a lamella will depend on the structure of the sample in the region being milled, the organoplatinum coat, and the time available. Ideally, the sample should be thinned until contrast is lost across the whole surface of the lamella by SEM at 3 kV, suggesting that it is evenly electron transparent and around 150–200 nm thick (**Figure 5C**). However, it may be necessary to stop milling before this point if the organoplatinum layer develops a hole or the lamella starts to bend. In this case, the lamella may still be thin enough at the front and remain useful for tomography. Conversely, it is possible to thin past the loss of

contrast stage if the lamella looks stable, making it even thinner by moving the milling patterns closer together (~100 nm or less). This will depend on what is required for the downstream workflow. It may require a low-magnification image to plan a polishing route, starting closer to the ions beam source and working away (**Figure 5D**). The direction of the polishing route is important to prevent redeposition of ablated material onto lamella that have already been finished.

Collecting and processing tilt-series data

Once loaded into the TEM, a low-magnification full grid montage (~150x) will identify the positions of the lamellae, which can be correlated to the low-magnification SEM image taken at the end of milling. For plunge frozen schizonts, most of the grid was not transparent to electrons, so the lamella positions appeared as white notches on a black background (**Figure 6A**). The angle of the lamellae with respect to the tilt axis of the microscope should be noted, as more than ~10° away from the perpendicular could make tilt-series acquisition difficult. A medium-magnification montage (~1,500x) at the location of each lamella will give an overview of the biological content and check for transfer damage, crystalline ice, or excessive surface contamination (**Figure 6B–D**). This should also be checked at high-tilt to ensure that no surface contamination obscures the acquisition or focus area. Choosing an acquisition region will depend not only on the biological features, but also the structural integrity of the ice in the surrounding region, for example, avoiding cracks, as these regions will drift, or areas with excessive curtaining, where a lamella will have variable thickness. Before acquiring a tilt-series, a ±0° pre-tilt is applied to the grid to make the plane of the lamellae (not the grid) perpendicular to the optical axis. The direction of the pre-tilt can be determined by the position of the front edge of the lamellae (looking for the left over organoplatinum coat) in the medium-magnification map. For the TEM used here (300 kV Titan Krios), if the front edges of the lamellae pointed up in the map, this required a +10° pre-tilt and if they pointed down, this required a -10° pre-tilt. Each grid may be different due to the orientation in which they were picked up in the tweezers and inserted into the autoloader (cutaway section facing left or right, produces a 180° rotation). A final consideration is pixel size. Routinely, tilt-series are collected around 2.5–7 Å/pixel, taking into account the size of the feature of interest, the target resolution of the resulting tomographic data and the surface area of the lamella, which may limit the size of acquisition area. It is possible to use a smaller pixel size to obtain high-resolution information and the smallest we have used successfully on these samples was 1.4 Å/pixel (data not shown). Drift will be more apparent at a smaller pixel size and is only really suitable for thin (<100 nm) lamellae where maximizing resolution is of importance in the study.

[Insert **FIGURE 6** here]

[Insert **FIGURE 7** here]

The primary focus of the work is to dissect the pathway of merozoite egress in *P. falciparum* but given that the population of cells used in the study can never be fully homogenous, often other stages of cell development within the lamellae were observed. The example shown here (**Figure 7**) contains a red blood cell that has recently been invaded by a *P. falciparum* parasite

(merozoite). The lamella used was 240 nm thick and the grid had been lightly sputter coated with platinum in an argon atmosphere prior to insertion into the TEM, resulting in slightly less contrast than would normally be expected. The red blood cell membrane could be traced in its entirety surrounding the cell. Within the red blood cell were three enclosed membrane-bound structures, two vesicles, each surrounded by a double membrane and a lightbulb-shaped feature (1.2 μm x 0.9 μm at its widest parts), which is consistent with it being a merozoite (**Figure 7A–B**). The contents of the two vesicles seemed to be similar in contrast to that of the contents of the red blood cell, suggesting that these vesicles may contain hemoglobin. The presence of vesicles within the host red blood cell after invasion has been observed previously⁴⁵. They are thought to arise from the secretion of lipids and other virulence factors from secretory organelles called rhoptries in the merozoite, which discharge into the host red cell during invasion. The merozoite is surrounded by two closely associated membranes, the inner-most of which is presumably the native plasma membrane of the merozoite, on which there is no visible surface coat, and the outer-most must derive from the host red cell membrane that envelopes the merozoite as it invades. The cytoplasm of the merozoite contains many multi-layered vesicles and an electron dense mushroom-shaped feature adjacent to a stack of membranes at the apex. A tilt-series acquired over this region (2.4 Å/pixel) shows that it contains a stack of four membranes, which appear to be connected to the mushroom-shaped feature (**Figure 7C–E**). Strikingly, this morphology is quite different to the normal arrangement of organelles and cellular structures in the apical end of a mature merozoite. To assess this, a comparative tilt-series (2.74 Å/pixel) over the apical end on a mature merozoite was obtained from a schizont that had been treated with E64 prior to plunge freezing and milling (**Figure 8**). This shows that the apical end of a merozoite contains two prominent club-shaped secretory organelles called rhoptries nestled within a set of three polar rings at the apical tip of the cell and surrounded by a number of smaller secretory organelles called micronemes. The inner-most polar ring is attached to a double membrane structure that underlies the merozoite plasma membrane, called the inner membrane complex, which contains motor proteins that drive invasion. It has been shown that during invasion the contents of the secretory organelles are discharged onto the merozoite surface and into the host red blood cell, facilitating attachment of merozoites to host red cells and initiating the motor complex that drives invasion⁴⁵. The data here shows that after invasion, the merozoite contains no observable structures that resemble rhoptries, micronemes, or polar rings, suggesting that the morphology of the apical end of the merozoite dramatically changes. Fusion of rhoptries prior to invasion has been shown previously by TEM of fixed, room temperature sections⁴⁶, which is consistent with the production of the mushroom-shaped feature we observe in our post-invasion state merozoite. The stacks of membranes connected to this feature have not been observed previously and since there is no indication of an IMC present in the newly invaded merozoite, we hypothesize that the membrane stacks may be the remnants of the IMC machinery left over after invasion is completed, but this remains to be confirmed.

[Insert **FIGURE 8** here]

FIGURES AND TABLES LEGENDS:

Table 1: Milling strategy to produce thin lamella. Step-wise milling is carried out by reducing the ion beam current corresponding to the thickness of the protected region. This limits sample heating, preventing devitrification. *Polishing should be performed in parallel to evenly apply heat to the lamellae from both sides, reducing the risk of them bending or bowing as they reach their final thickness. Other steps can be done sequentially, milling the pattern above the lamella and then below the lamella, before moving to the next beam current. Surveying the grid to locate milling positions should be carried out at 1.5 pA beam current to minimize sample heating.

Figure 1: The morphology of compound 2 and E64-stalled *P. falciparum* schizonts by Giemsa-stained blood smears. (A) In the presence of compound 2 the parasitophorous vacuole (PV) is densely packed with merozoites (purple circles) with a single cluster of hemozoin crystals (dark brown circle). The boundary between the PV and the surrounding hemoglobin in the host red blood cell (hRBC) (grey band) is well defined, as well as the hRBC membrane. (B) In the presence of E64, the PV membrane is ruptured and the merozoites spread out within the hRBC. Each schizont still contains a single cluster of hemozoin crystals. The host cell membrane is leaky and partially collapses, therefore, no hemoglobin is visible within cell periphery and the boundary of the hRBC membrane is not easily visible. Scale bar, 5 μm .

Figure 2. Analyzing the cell distribution on grids of plunge frozen *P. falciparum* schizonts by cryo-light microscopy. (A) An example of ice being too thick across a grid square by cryo-light microscopy, obscuring the cells and the carbon film. Scale bar, 10 μm . (B) An example of the hole size (300 mesh copper grid with 5/2 square holey carbon film) being too big for the cells, resulting in a very thin layer of biological material surrounded by empty regions with no ice. Grids such as this produce very short, unstable lamellae. Scale bar, 10 μm . (C) An example of good cell distribution on a 200-mesh copper grid with 2/4 holey carbon film. These schizonts were treated with E64 inhibitor. The large cells (red box, $\sim 5 \mu\text{m}$ diameter) with a well-defined periphery are infected red blood cells that still have an intact vacuole membrane. The clusters of small cells (blue box, $\sim 1 \mu\text{m}$) are the individual merozoites contained within a partially collapsed host red blood cell. Each schizont has a black spot at its center, indicating the position of the hemozoin crystals (See **Figure 1** for additional details). The difference in cell morphology is not as easy to see once inside the cryoFIB-SEM; therefore, pre-screening by cryo-light microscopy is beneficial until reproducible blotting conditions have been reached. The cell coverage around the edges of the grid square next to the grid bars (white-dashed areas) is too thick for milling. The thinner region in the center of the grid square (yellow-dashed area) is an ideal place to mill from, extending the lamella into the surrounding layer of cells. Scale bar, 6 μm . (D) Image of a cryoFIB-specific autogrid rim with two black marks, one within the cutaway section (black bracket) and the other opposite, at 12 o'clock and 6 o'clock. The black arrow represents the milling direction. (E) When the grids are loaded into the autoloader cassette, the marks need to be equidistant either side of the loading tweezers, resulting in the lamellae lying perpendicular to the tilt axis of the stage.

Figure 3: A good quality organoplatinum coating is critical to obtain thin, evenly milled lamellae. (A) A micrograph of the front edge of a lamella where the organoplatinum coating

(OP, yellow) has been applied too thinly, leading to a hole in the front edge of the lamella that developed during polishing (green circle) and uneven milling across the whole width of the lamella (streaks). The organoplatinum surface has been sheared off by the ion beam, leading to a spray of material behind the front edge of the coating (yellow-dashed line). (B) The organoplatinum coat (OP) has been applied more thickly, resulting in a more evenly thinned lamella. The integrity of the coat is preserved across the entire width of the lamella and the interface between the organoplatinum coat and the vitrified biological material is well defined (yellow-dashed line). The carbon layer can be seen running through the rear of the lamella (orange). Scale bars, 1 μm .

Figure 4: Assessing grid quality and locating areas to mill in the cryoFIB-SEM. (A) A low-magnification overview of a grid at 5 kV via the SEM. The cutaway section of the autogrid rim is visible at the bottom of the image. Scale bar, 0.5 mm. (B) The same grid at 30 kV by SEM, showing areas of thicker ice (darker grid squares) and thinner ice (lighter grid squares). The inset shows the region in the box, with arrows indicating the numbering on the finder grid, which is visible at 30 kV. Scale bar, 0.5 mm. (C) A medium-magnification overview of two grid squares assessing the distribution of the cells on the carbon film and location of the grid bars. Scale bar, 50 μm . (D) The arrangement of milling patterns for the first cut at high-magnification (ion beam view at 1.5 pA and 30 kV). The red region (3 μm thick) is protected, while the yellow regions will be ablated by the ion beam. The white-dashed line indicates the position of the final lamella. Scale bar, 10 μm . (E) A high-magnification view at 3 kV via the SEM of a polished 200 nm thick lamella (10 μm wide x 15 μm long). The loss of contrast within the lamella at 3 kV indicates that a suitable thickness has been reached. The bright-white front edge is the remaining organoplatinum layer that is applied to the grid via the GIS prior to milling. Scale bar, 5 μm . (F) The same lamella from (E) viewed using the ion beam at 30 kV and 1.5 pA. The thin white line across the black square (white arrow) is the remaining organoplatinum coat on the very front edge of the lamella. Scale bar, 10 μm .

Figure 5: Determining when final lamella thickness has been reached during milling. (A) Low-magnification overview of a grid by SEM at 5 kV showing carbon damage during clipping. The undamaged areas contained very thin sample due to over-blotting; however, it was still possible to mill six lamellae on this grid (the region within the white-dashed outline) in a full day session on the cryoFIBSEM. Scale bar, 0.5 mm. (B) A short lamella (~10 μm wide x 3 μm long, not including organoplatinum layer) produced from this grid (SEM at 3 kV), which still provided two regions from which to collect tilt-series. Scale bar, 25 μm . (C) A series of SEM images (3 kV) of a lamella during the final polishing step showing how contrast is lost in the lamella as it is thinned (moving left to right). The dark black line across the middle of the lamella in all images is a strip of carbon film from the grid. Cells in front of this region were vitrified above the carbon film and cells behind this region were vitrified below the carbon film. Milling was stopped when the organoplatinum coat on the left side of the front edge of the lamella was near to losing structural integrity. This stopping point was before the entire lamella was brought to an even thickness, which is why there is still some higher contrast material in the rear of the lamella. (D) An example of a polishing route based on the lamellae milled on the grid shown in (A). A polishing route should start at lamellae nearer the FIB source, moving away from the FIB source

to limit redeposition of milled material onto the surface of the lamellae.

Figure 6: Choosing accessible regions of interest from which to acquire tilt-series (A) A section of a low-magnification TEM map showing a region containing lamellae, appearing as six white notches on a black background (red arrows). The white squares are broken carbon film. (B) A medium-magnification map of a damaged and devitrified lamella. At the front edge of the lamella (FE) the organoplatinum coat has snapped off (1). There is a clear patch of crystalline ice in the center of the lamella (2). The ion beam has failed to break through at the back edge of the lamella (BE) because the ice is too thick next to the grid bars. Only a small portion of the lamella is free from the surrounding ice at the BE (3), creating a wedge. The thickness has also caused shelves to be cut above the lamella (4), which will most likely block the view of the cells at high-tilt in the TEM. (C) Medium-magnification montage of a whole lamella viewed in the TEM. Typical problems or regions to be avoided when collecting tilt-series from lamellae are areas: covered with surface contamination (SC), covered by the organoplatinum coat (OP, yellow), near cracks (CR and black arrows), with curtaining due to density changes in biological material (CU and region within blue brackets), and areas weakened by breaks in the organoplatinum coat (green circle). The only regions accessible for tilt-series acquisition are the areas within the two black-dashed boxes (labeled 1 and 2). The view must be checked at high-tilt to make sure surface contamination does not obscure the region of interest or the focus area. (D) A medium-magnification montage of a much cleaner lamella, but which still has cracks (CR) caused by thinning of the organoplatinum coat (green circle) during polishing. Here, the region of interest is highlighted by the cell type observed within the lamella, which in this case are the individual merozoites, positioned behind the carbon layer (orange) toward the rear of the lamella (black-dashed box). Scale bars, 3 μm .

Figure 7: Acquiring cryo-ET data from FIB-milled lamella. (A) A micrograph of a region of a lamella containing a red blood cell that has recently been invaded by a *P. falciparum* merozoite. In (B) the same image is annotated to show the boundary of the red blood cell (red), a number of double-walled intracellular vesicles (purple and blue for the inner and outer membranes, respectively) and the merozoite (green) surrounded by a second membrane derived from the host cell (yellow). A black box shows the area where a tilt-series was acquired. Scale bar, 500 nm. (C) An average of 20 central slices viewed in the XY plane from an 8x binned tomogram (2.4 $\text{\AA}/\text{pixel}$) acquired at the apical end of the merozoite and in (D) its annotation, showing the two membranes surrounding the cell (green and yellow) and four membranes stacked in the apex of the merozoite (blue) that are associated with an electron dense mushroom-shaped feature (purple). A red arrow indicates the junction of the membrane stacks in the apex and the mushroom-shaped feature (also shown in part F, i). A black arrow indicates a fusion event between the merozoite plasma membrane and one of the multi-layered vesicles within the parasite (also shown in part F, ii). The host red blood cell membrane is shown (red) and a black-dashed line shows the position of a cross-section viewed in the XZ plane, shown in (E). The features in the cross-section (E) are colored and labeled the same as in part (D), with colored arrows pointing to the membranes. A black arrow indicates the position of a sputter coat applied to the lamella after milling and the thickness of the lamella is indicated. For parts (C–E), scale bar, 500 nm. (F) A more detailed view of the features indicated by the red and black arrow

heads in part (C), showing the definition in the lipid bi-layers of the membrane stack in the apex of the merozoite (i) and the fusion event between the multi-layered vesicle with the merozoite plasma membrane. Scale bar, 75 nm.

Figure 8: The apical end of mature merozoites by cryo-ET of a FIB-milled lamella and TEM of plastic sections. (A) An average of 20 central slices from an 8x binned tomogram (2.74 Å/pixel) from a 230 nm thick lamella showing the typical morphology of the apical end of a mature merozoite. The schizonts were treated with E64 prior to plunge freezing, thus the PV membrane has ruptured and the merozoites are contained within the host red cell. (B) shows the same as in (A), but with annotations to indicate the host red blood cell membrane (RCM, red), the merozoite plasma membrane (green), the inner membrane complex (IMC, purple), polar rings (PR, black), micronemes (M, yellow), rhoptries (R, grey), and the nuclear envelope (NE, blue). A neighboring merozoite, which is out of plane in this region of tomogram is indicated by a green triangle. Scale bar, 200 nm. (C) The cellular features observed by cryoET are consistent with those from TEM of schizonts preserved in plastic sections. Similar cellular features are indicated in a mature merozoite from a schizont that has been treated with compound 2, stalling egress prior to PV membrane rupture. Scale bar, 500 nm. (D) An annotated schematic of a merozoite showing the cellular features in parts (A–C).

DISCUSSION:

While cryoFIB-milling is becoming more routine, preparation of optimal samples for milling has not; therefore, most of the critical steps in this protocol occur before the sample reaches the cryoFIB-SEM. Sample optimization by multiple rounds of cell preparation, plunge freezing, and screening by light and electron microscopy are required to produce the best possible sample before milling is attempted. Having the best sample possible not only increases the chances of success but also optimizes the use of the equipment. For this reason, most national facilities require evidence that sufficient optimization has been carried out before granting time on their machines. Once inside the cryoFIB-SEM, maximizing the effectiveness of the organoplatinum coat is critical in order to produce uniformly thin lamellae. Finally, patience and good sample handling is a prerequisite skill from the user, who will be required to sit for multiple days producing and then transferring grids containing delicate lamellae. This may change with the introduction of automated milling strategies^{47–48}, but as yet, the entire milling process is still largely manual at most facilities.

While the work focused solely on *P. falciparum* schizonts, the method presented here could be easily modified to optimize grid preparation and milling for other cell types. Important factors to consider are the density of the cells being applied to the grid, the grid type (copper is toxic to some cells), the size and spacing of holes in the carbon film, the blotting time, and the method of blotting (single/double sided, manual, or automated). Additionally, if the cells are being grown on the grids (usually gold grids with a holey carbon film), confluency can be checked by light microscopy before blotting and freezing. The milling strategy depends on how the cells are deposited on the grid. For malaria infected red blood cells, the grid is essentially coated by an unbroken layer of cells, thicker in some areas and thinner in other areas. Milling is carried out at multiple points at one region along this gradient where the ice thickness generates lamellae

that are a suitable size for tomography. This approach works well for smaller cells as you can produce lamellae containing a slice through multiple cells. For larger cells or clumps of cells, it might be the case that one cell or cell clump may produce one lamella.

Grid handling and sample transfer remain one of the main challenges of this workflow. Lamellae can be lost due to breakages or cracks, curtaining artefacts obscuring the biology, excessive surface contamination, as well as grid orientation problems within the TEM, requiring an extra handling step to reposition the grid. The degree of losses varies from day-to-day and grid-to-grid, but it is improved through practice and handling experience over time. It was found that the grids can be carefully reorientated in the autoloader multiple times without destroying lamellae and this sometimes has the benefit of washing off surface ice. Another main limitation of this workflow is the time it takes to produce lamellae. As production is slow, it is critical to have a properly optimized sample, making the milling as efficient as possible.

A number of adaptations to FIB-milling of vitreous biological samples have recently been introduced. A game-changer is the implementation of cryogenically cooled lift-out tools within the cryoFIB-SEM chamber that enable larger blocks of material to be milled from high-pressure frozen samples. The blocks can be attached to a metal rod or picked up in a gripper and moved to a second sample position, containing a specially modified EM grid. The blocks can then be coated with organoplatinum and milled to generate lamellae. The ability to mill lamellae from high-pressure frozen material means that much larger cells and tissues can be processed, specifically targeting areas by correlative fluorescence microscopy¹². Other recent adaptations to the FIB-milling method include reducing curtaining artifacts by wedge pre-milling the sample¹⁶, microfluidic cryo-fixation⁴⁹ and photo-micropatterning of electron microscopy grids to improve cell distribution⁵⁰. Also, it has been demonstrated that milling micro-expansion gaps either side of a lamella can alleviate compression by the surrounding sample as it reaches its final thinness⁵¹. This may be particularly useful when milling continuous cell layers, such as the sample in this study, where bending of lamellae is sometimes seen during the final polishing step.

The future of electron microscopy will likely be the determination of *in situ* molecular structures by sub-tomogram averaging and FIB-milling is an important tool that will facilitate the production of vitreous biological samples for these types of workflows. While FIB-milling is still in its infancy for biological applications, methods development is happening at a rapid pace thanks to the hard work of researchers, both academic and at national facilities, plus commercial investment in developing cryoFIB-SEM technology to support research.

ACKNOWLEDGMENTS:

This project for which this method was developed was funded by a Medical Research Council grant MR/P010288/1 awarded to Helen R. Saibil and Michael J. Blackman. Cultures of *P. falciparum* were grown at The Francis Crick Institute, with the support of members of Michael J. Blackman's group. The authors would like to thank Dr. Ser Ying (Michele) Tan for providing the images of compound 2 and E64-treated schizonts in thin blood smears. Most of the lamellae were produced with support from staff at eBIC and we are grateful for access to the Scios dual-

beam cryoFIB-SEM on research proposal NT21004. The authors also acknowledge the support of the Royal Society Industry Fellowship scheme (INF\R2\202061) and Wellcome Trust Multi-user Equipment Grant (212916/Z/18/Z) in continuing the development of the FIB-milling technique within the CUI. The authors would also like to thank Helen R. Saibil for useful discussions in relation to this methods paper and supervising the project.

DISCLOSURES:

The authors have nothing to disclose.

REFERENCES:

1. Baumeister, W. From proteomic inventory to architecture. *FEBS Letters*. **579** (4), 933–937 (2005).
2. Rigort, A., Villa, E., Bäuerlein, F. J. B., Engel, B. D., Plitzko, J. M. Integrative approaches for cellular cryo-electron tomography: Correlative imaging and focused ion beam micromachining. *Methods in Cell Biology*. **111**, 259–281 (2012).
3. Oikonomou, C. M., Chang, Y. W., Jensen, G. J. A new view into prokaryotic cell biology from electron cryotomography. *Nature Reviews Microbiology*. **14**, 205–220 (2016).
4. Wagner, F. R. et al. Preparing samples from whole cells using focused-ion-beam milling for cryo-electron tomography. *Nature Protocols*. **15** (6), 2041–2070 (2020).
5. Giannuzzi, L. A., Stevie, F. A. A review of focused ion beam milling techniques for TEM specimen preparation. *Micron*. **30** (3), 197–204 (1999).
6. Narayan, K., Subramaniam, S. Focused ion beams in biology. *Nature Methods*. **12** (11), 1021–1031 (2015).
7. Rigort, A. et al. Focused ion beam micromachining of eukaryotic cells for cryoelectron tomography. *Proceedings of the National Academy of Science of the United States of America*. **109** (12), 4449–4454 (2012).
8. Marko, M., Hsieh, C., Schalek, R., Frank, J., Mannella, C. Focused-ion-beam thinning of frozen-hydrated biological specimens for cryo-electron microscopy. *Nature Methods*. **4** (3), 215–217 (2007).
9. Villa, E., Schaffer, M., Plitzko, J. M., Baumeister, W. Opening windows into the cell: Focused-ion-beam milling for cryo-electron tomography. *Current Opinion in Structural Biology*. **23** (5), 771–777 (2013).
10. Wang, K., Strunk, K., Zhao, G., Gray, J. L., Zhang, P. 3D structure determination of native mammalian cells using cryo-FIB and cryo-electron tomography. *Journal of Structural Biology*. **180** (2), 318–326 (2015).
11. de Winter, D. A. M. et al. In-situ integrity control of frozen-hydrated, vitreous lamellas prepared by the cryo-focused ion beam-scanning electron microscope. *Journal of Structural Biology*. **183** (1), 11–18 (2013).
12. Schaffer, M. et al. A cryo-FIB lift-out technique enables molecular-resolution cryo-ET within native *Caenorhabditis elegans* tissue. *Nature Methods*. **16** (8), 757–762 (2019).
13. Mahamid, J. et al. Visualizing the molecular sociology at the HeLa cell nuclear periphery. *Science*. **351** (6276), 969–972 (2016).
14. Albert, S. et al. Proteasomes tether to two distinct sites at the nuclear pore complex. *Proceedings of the National Academy of Science of the United States of America*. **114** (52),

13726–13731 (2017).

15. Guo, Q. et al. In situ structure of neuronal C9orf72 poly-GA aggregates reveals proteasome recruitment. *Cell*. **172** (4), 696–705 (2018).
16. Schaffer, M. et al. Optimized cryo-focused ion beam sample preparation aimed at in situ structural studies of membrane proteins. *Journal of Structural Biology*. **197** (2), 73–82 (2017).
17. Szwedziak, P., Wang, Q., Bharat, T. A. M., Tsim, M., Löwe, J. Architecture of the ring formed by the tubulin homologue FtsZ in bacterial cell division. *eLife*. **3**, e04601 (2014).
18. Carlson, L., A. et al. Cryo electron tomography of native HIV-1 budding sites. *PLOS Pathogens*. **6** (11), e1001173 (2010).
19. Klein S. et al. SARS-CoV-2 structure and replication characterized by in situ cryo-electron tomography. *Nature Communications*. **11** (1), e5885 (2020).
20. Studer, D., Humbel, B. M., Chiquet, M. Electron microscopy of high pressure frozen samples: Bridging the gap between cellular ultrastructure and atomic resolution. *Histochemistry and Cell Biology*. **130** (5), 877–889 (2008).
21. Schertel, A. et al. Cryo FIB-SEM: Volume imaging of cellular ultrastructure in native frozen specimens. *Journal of Structural Biology*. **184** (2), 355–360 (2013).
22. Murphy, G. E. et al. Correlative 3D imaging of whole mammalian cells with light and electron microscopy. *Journal of Structural Biology*. **176** (3), 268–278 (2012).
23. Heymann, J. A. W. et al. Site-specific 3D imaging of cells and tissues with a dual beam microscope. *Journal of Structural Biology*. **155** (1), 63–73 (2012).
24. Spehner D. et al. Cryo-FIB-SEM as a promising tool for localizing proteins in 3D. *Journal of Structural Biology*. **211** (1), e107528 (2020).
25. Kamino, T., Yaguchi, T., Ohnishi, T., Ishitani, T., Osumi, M. Application of a FIB-STEM system for 3D observation of a resin-embedded yeast cell. *Journal of Electron Microscopy* (Tokyo). **53** (5), 563–566 (2004).
26. Han, H., Zuber, B., J. Dubochet. Compression and crevasses in vitreous sections under different cutting conditions. *Journal of Microscopy*. **230** (Pt 2), 167–171 (2008).
27. Matias, V. R. F., Al-amoudi, A., Dubochet, J., Beveridge, T. J. Cryo-transmission electron microscopy of frozen-hydrated sections of *Escherichia coli* and *Pseudomonas aeruginosa*. *Journal of Bacteriology*. **185** (20), 6112–6118 (2003).
28. Al-Amoudi, A., Studer, D., Dubochet, J. Cutting artefacts and cutting process in vitreous sections for cryo-electron microscopy. *Journal of Structural Biology*. **150** (1), 109–121 (2005).
29. Al-Amoudi, A. et al. Cryo-electron microscopy of vitreous sections. *The EMBO Journal*. **23** (18), 3583–3588 (2004).
30. Bouchet-Marquis, C., Dubochet, J., Fakan, S. Cryoelectron microscopy of vitrified sections: A new challenge for the analysis of functional nuclear architecture. *Histochemistry and Cell Biology*. **125** (1–2), 43–51 (2006).
31. Hayles, M. F. et al. The making of frozen-hydrated, vitreous lamellas from cells for cryo-electron microscopy. *Journal of Structural Biology*. **172** (2), 180–190 (2010).
32. Dubochet, J., Adrian, M., Chang, J.-J., Lepault, J., McDowell, A. W. Cryoelectron microscopy of vitrified specimens. *Cryotechniques in Biological Electron Microscopy*. Springer, Berlin Heidelberg. 114–131 (1987).
33. Hsieh, C., Schmelzer, T., Kishchenko, G., Wagenknecht, T., Marko, M. Practical workflow for cryo focused-ion-beam milling of tissues and cells for cryo-TEM tomography. *Journal of*

881 *Structural Biology*. **185** (1), 32–41 (2014).

882 34. Harapin, J. et al. Structural analysis of multicellular organisms with cryo-electron
883 tomography. *Nature Methods*. **12** (7), 634–636 (2015).

884 35. Rubino, S. et al. A site-specific focused-ion-beam lift-out method for cryo Transmission
885 Electron Microscopy. *Journal of Structural Biology*. **180** (3), 572–576 (2012).

886 36. Duyvesteyn, H. M. E. et al. Machining protein microcrystals for structure determination
887 by electron diffraction. *Proceedings of the National Academy of Science of the United States of*
888 *America*. **115** (38), 9569–9573 (2018).

889 37. Blackman, M. J. Purification of *Plasmodium falciparum* merozoites for analysis of the
890 processing of merozoite surface protein-1. *Microbes as Tools for Cell Biology*. Academic Press,
891 London, UK. **45**, 213–220 (1995).

892 38. Hagen, W. J. H., Wan, W., Briggs, J. A. G. Implementation of a cryo-electron tomography
893 tilt-scheme optimized for high resolution subtomogram averaging. *Journal of Structural Biology*.
894 **197** (2), 191–198 (2017).

895 39. Zheng, S. Q. et al. MotionCor2 - anisotropic correction of beam-induced motion for
896 improved cryo-electron microscopy. *Nature Methods*. **14** (4), 331–332 (2017).

897 40. Grant, T., Grigorieff, N. Measuring the optimal exposure for single particle cryo-EM using
898 a 2.6 Å reconstruction of rotavirus VP6. *eLife*. **4**, e06980 (2015).

899 41. Rohou, A., Grigorieff, N. CTFFIND4: Fast and accurate defocus estimation from electron
900 micrographs. *Journal of Structural Biology*. **192** (2), 216–221 (2015).

901 42. Kremer, J. R., Mastronarde, D. N., McIntosh, J. R. Computer visualization of three-
902 dimensional image data using IMOD. *Journal of Structural Biology*. **116** (1), 71–76 (1996).

903 43. Turoňová, B., Schur, F. K. M., Wan, W., Briggs, J. A. G. Efficient 3D-CTF correction for
904 cryo-electron tomography using NovaCTF improves subtomogram averaging resolution to 3.4 Å.
905 *Journal of Structural Biology*. **199** (3), 187–195 (2017).

906 44. Arnold, J. et al. Site-specific cryo-focused ion beam sample preparation guided by 3d
907 correlative microscopy. *Biophysical Journal*. **110** (4), 860–869 (2016).

908 45. Riglar, D. T. et al. Super-resolution dissection of coordinated events during malaria
909 parasite invasion of the human erythrocyte. *Cell Host & Microbe*. **9** (1), 9–20 (2011).

910 46. Hanssen, E. et al. Electron tomography of *Plasmodium falciparum* merozoites reveals
911 core cellular events that underpin erythrocyte invasion. *Cellular Microbiology*. **15** (9), 1457–
912 1472 (2013).

913 47. Buckley, G. et al. Automated cryo-lamella preparation for high-throughput in-situ
914 structural biology. *Journal of Structural Biology*. **210** (2), 107488 (2020).

915 48. Zachs, T. et al. Fully automated, sequential focused ion beam milling for cryo-electron
916 tomography. *eLife*. **9**, e52286 (2020).

917 49. Fuest, M. et al. In situ microfluidic cryofixation for cryo focused ion beam milling and
918 cryo electron tomography. *Scientific Reports*. **9** (1), 19133 (2019).

919 50. Toro-Nahuelpan, M. et al. Tailoring cryo-electron microscopy grids by photo-
920 micropatterning for in-cell structural studies. *Nature Methods*. **17** (1), 50–54 (2020).

921 51. Wolff, G. et al. Mind the gap: Micro-expansion joints drastically decrease the bending of
922 FIB-milled cryo-lamellae. *Journal of Structural Biology*. **208** (3), 107389 (2019).

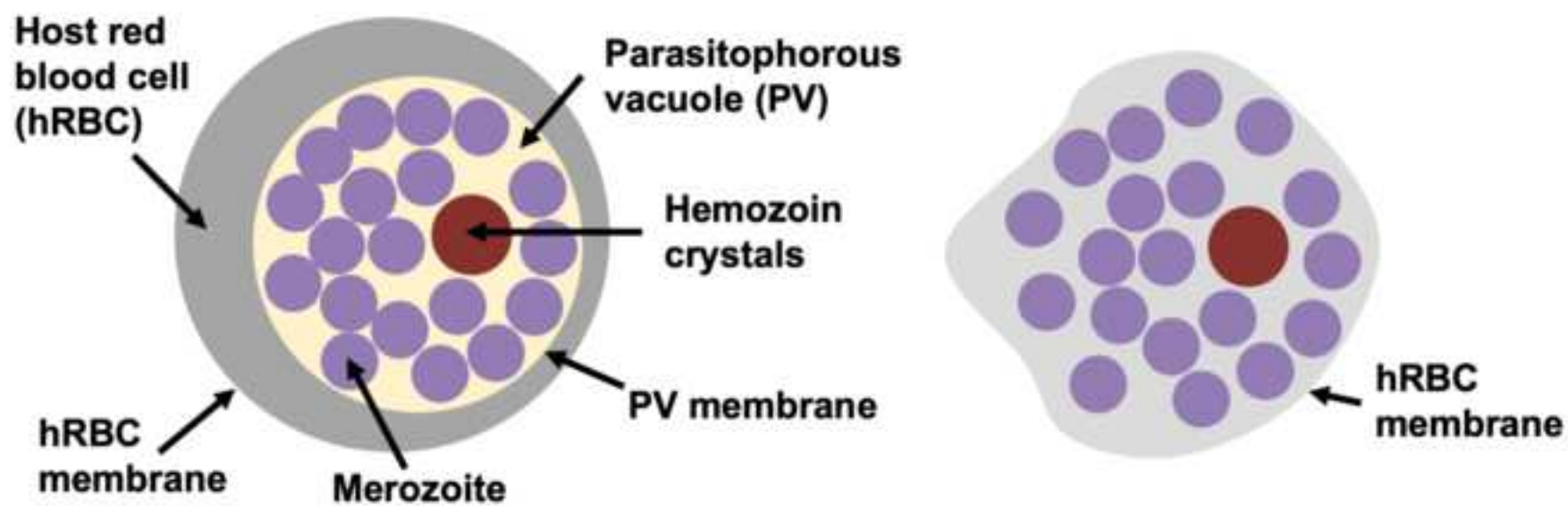
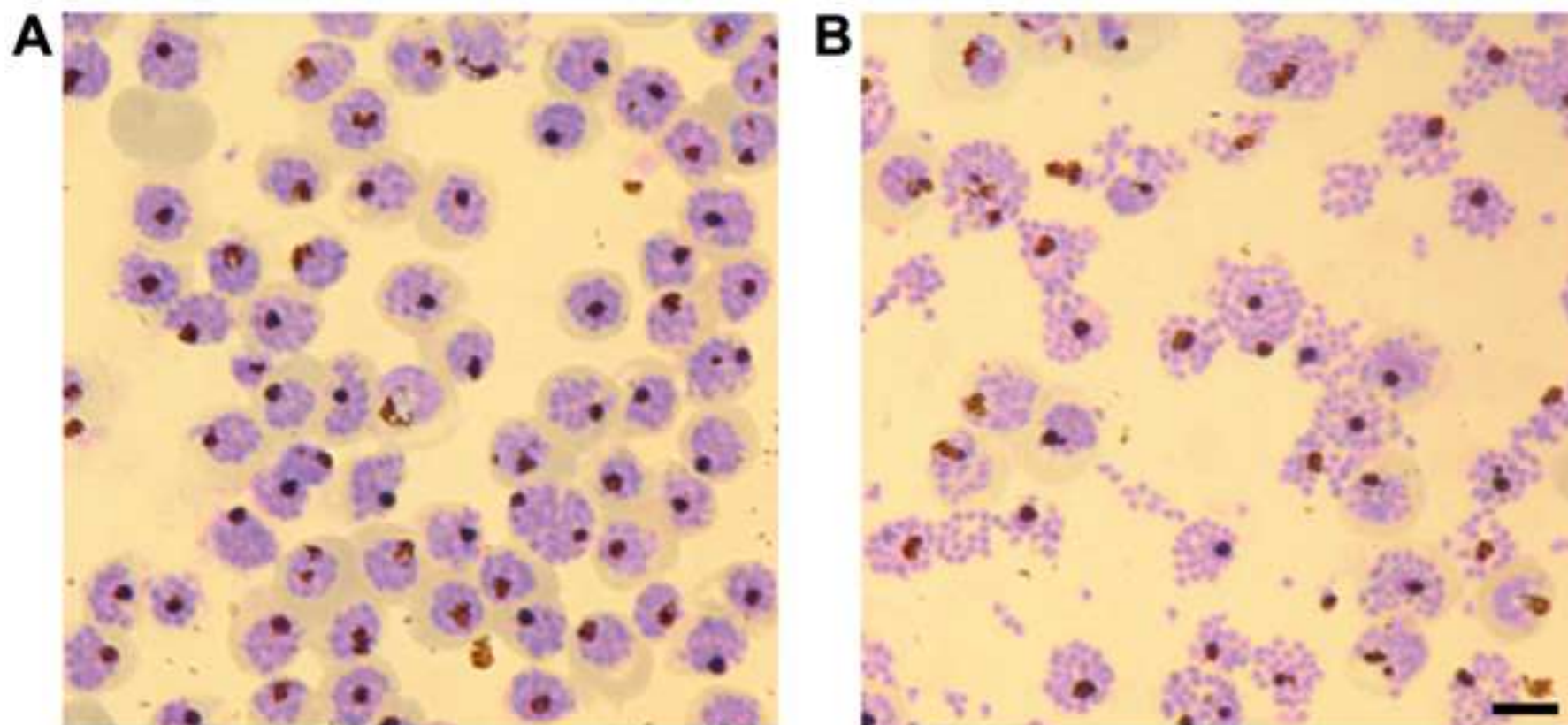
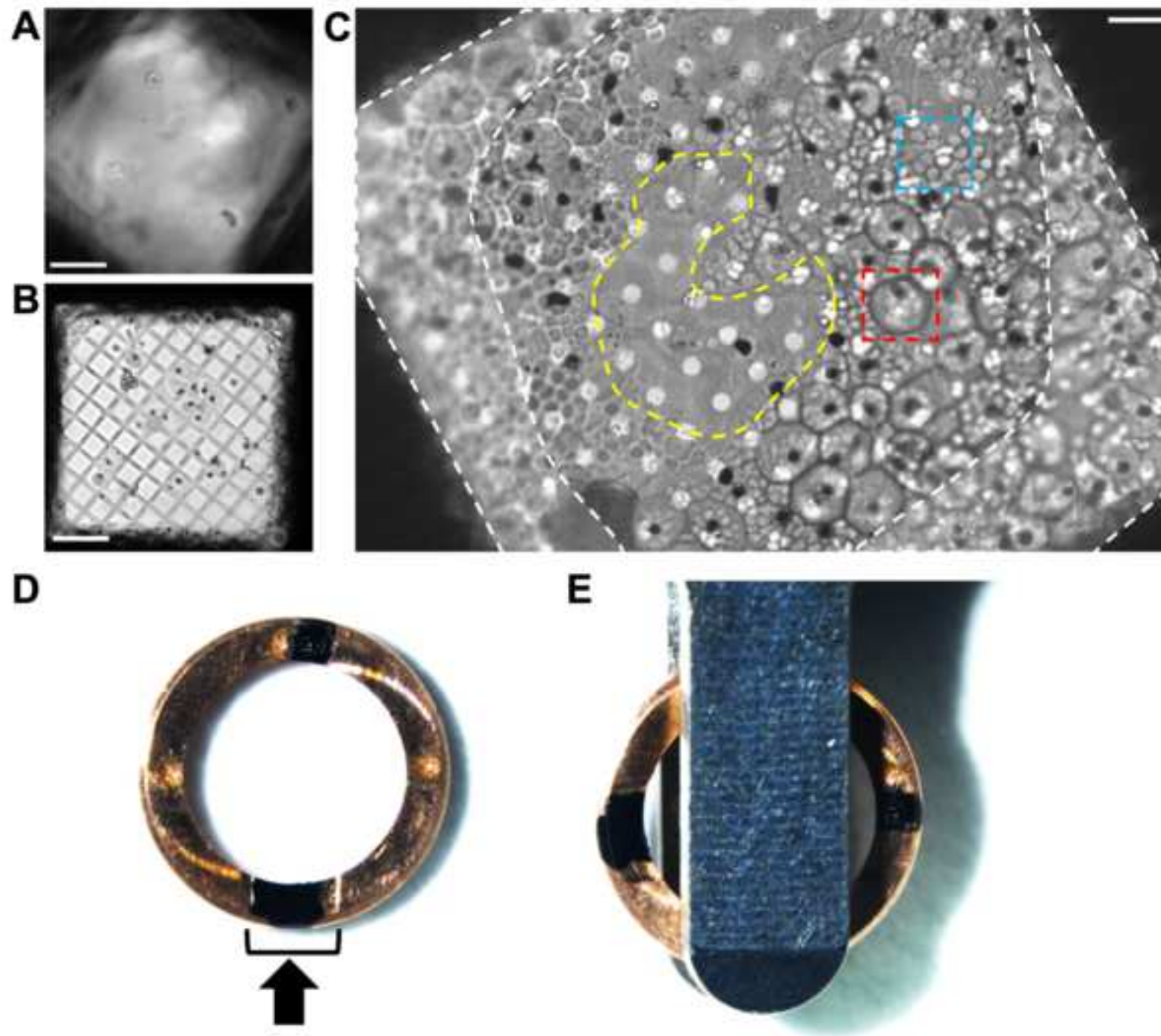
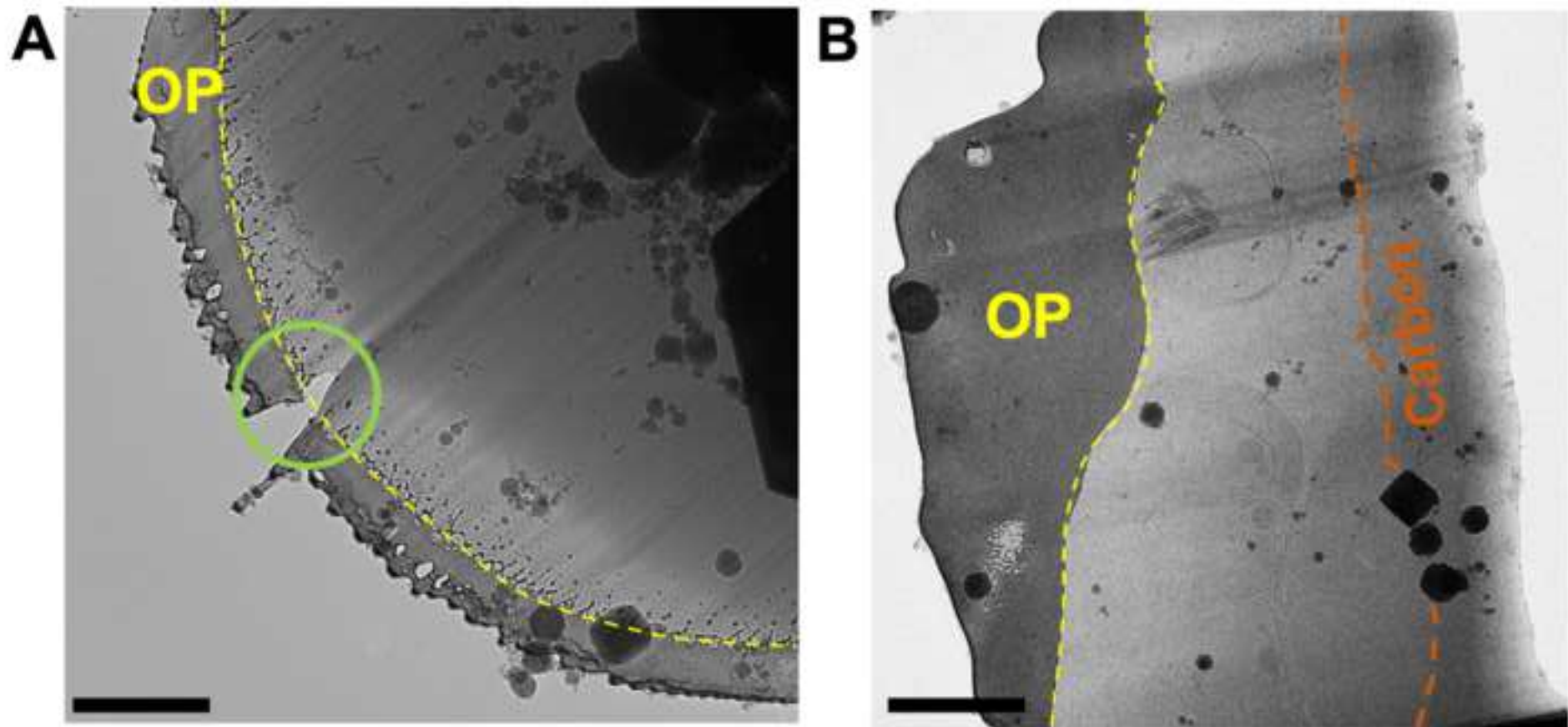
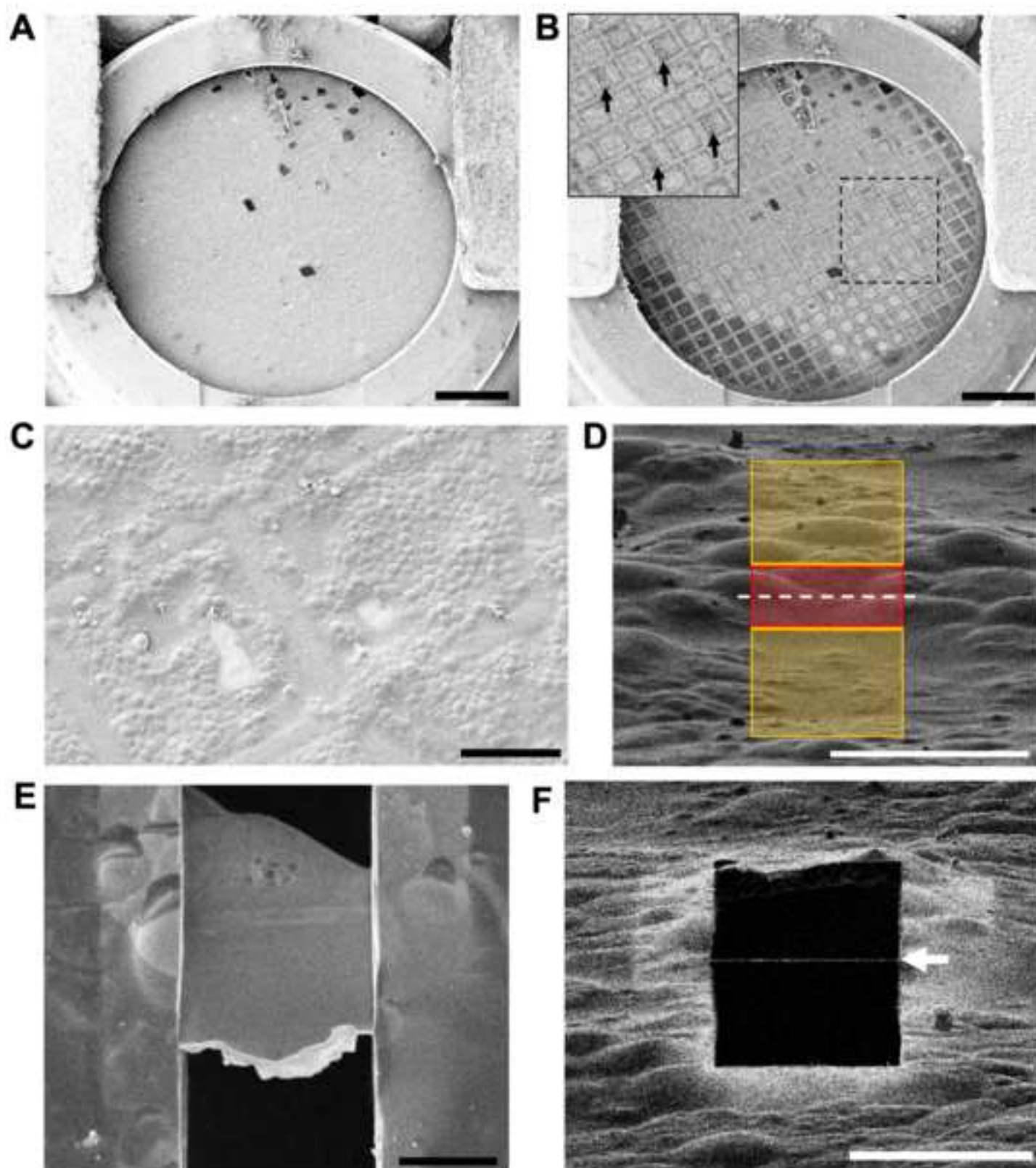


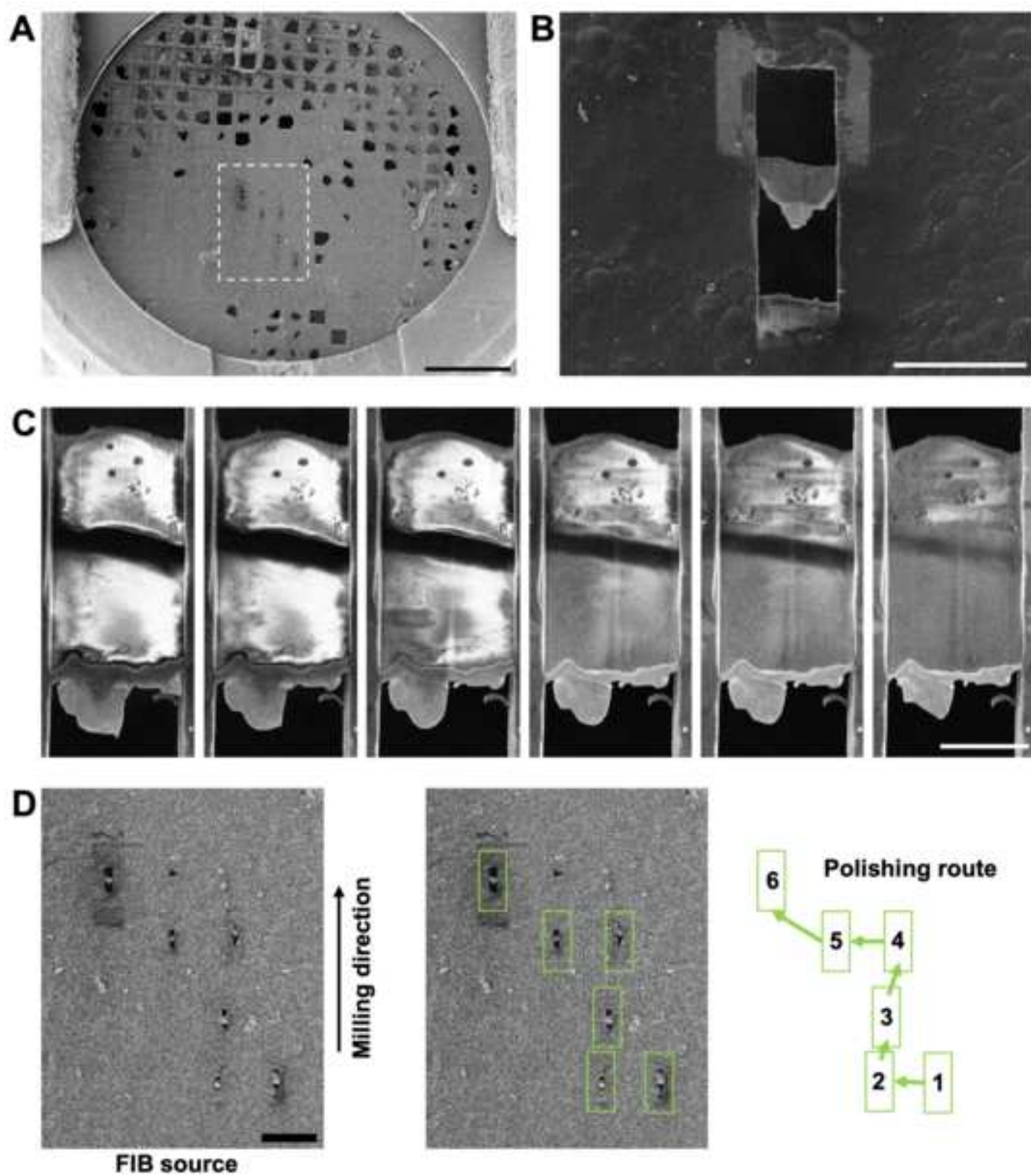
Figure 2

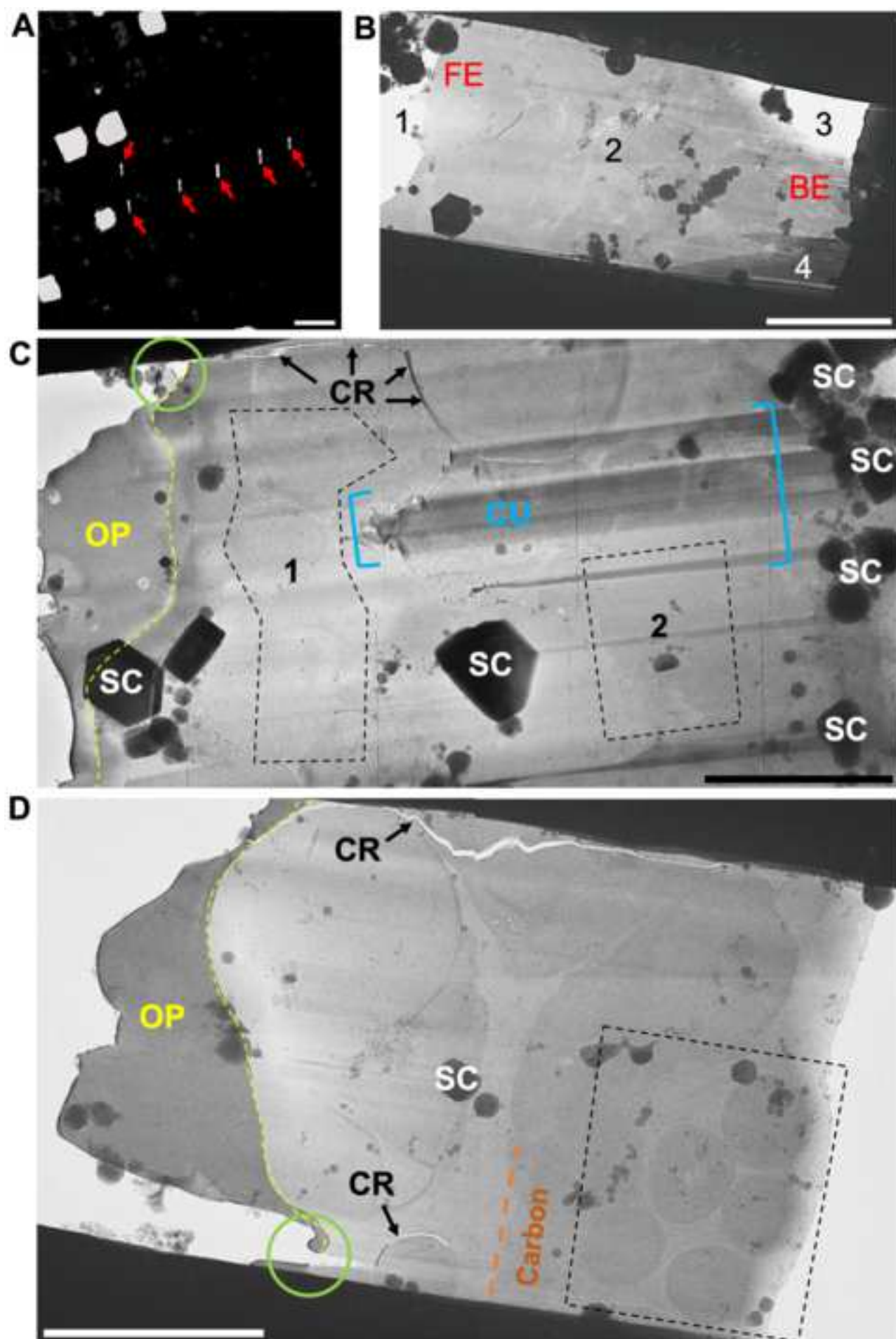
[Click here to access/download;Figure;figure2.tiff](#)

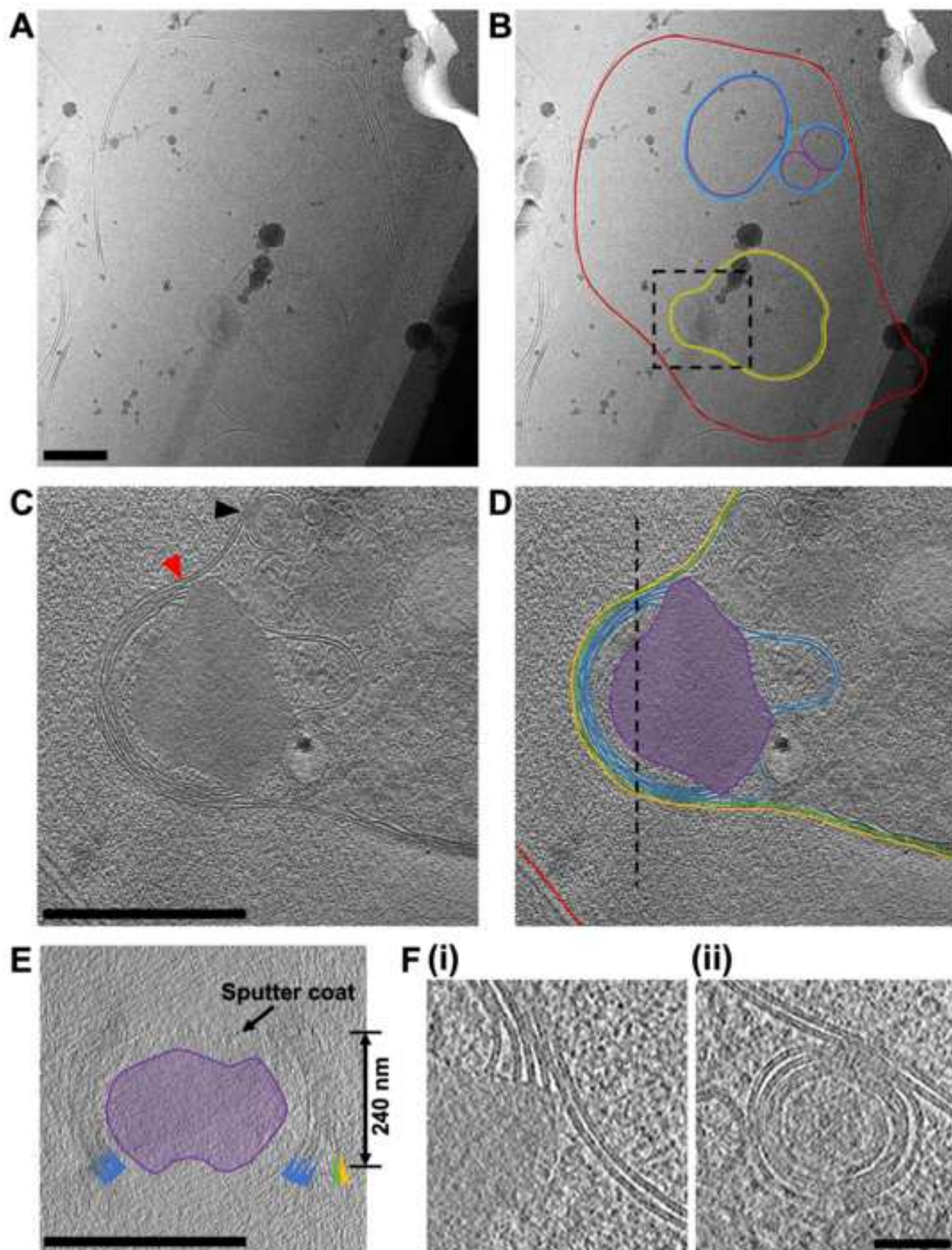


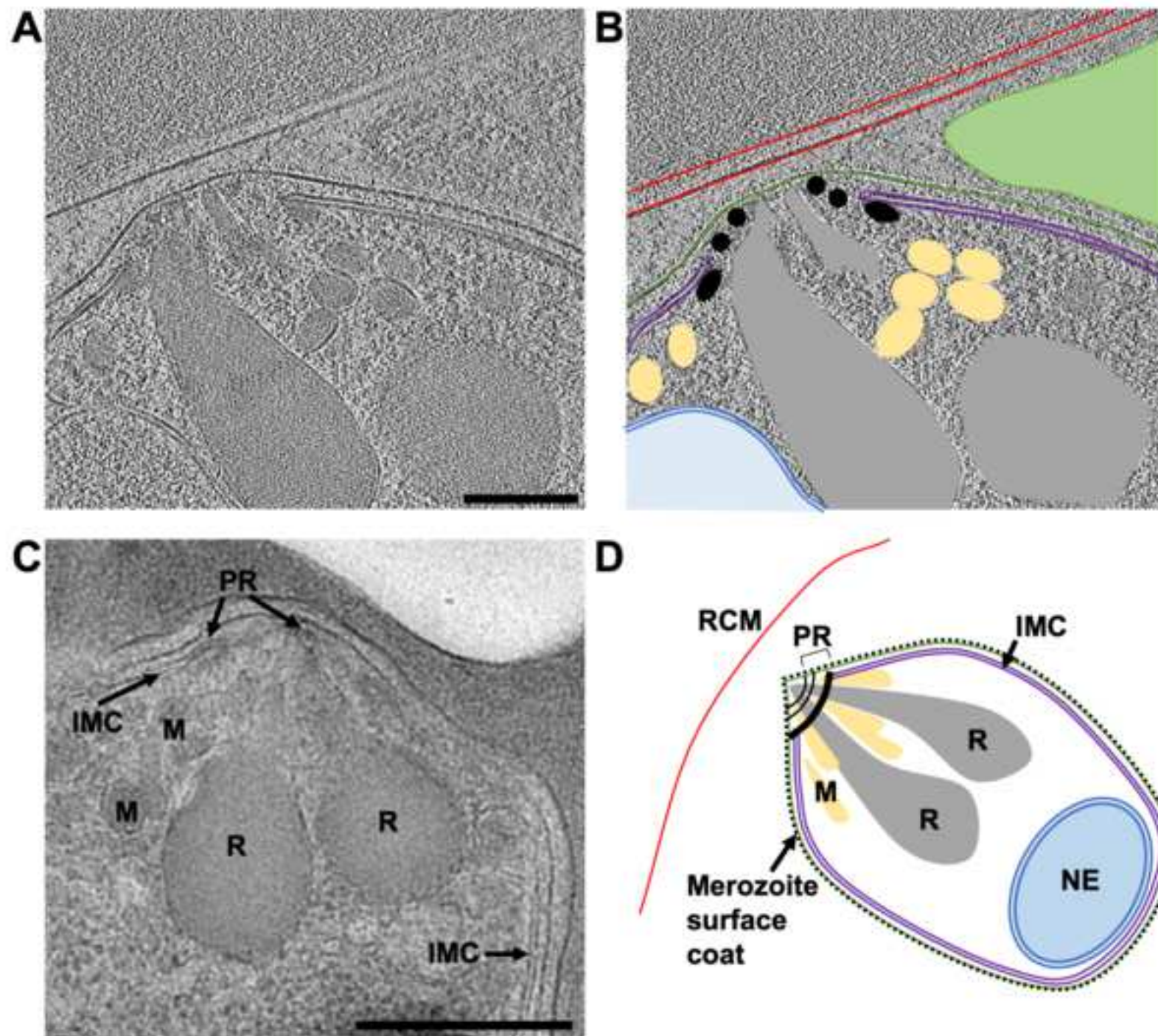












| Thickness of protected region between the rectangular milling patterns (μm) | Nominal ion beam current (pA) at 30 kV |
|--|--|
| 3 | 300 |
| 1.5 | 100 |
| 0.75 | 50 |
| 0.3 | 30 |
| 0.2 – 0.06 (final polishing) | 30* |

| Name of Material/Equipment | Company | Catalog Number |
|--|--------------------------|------------------|
| c-clips | Thermo Fisher Scientific | 1036171 |
| Clipping station | Thermo Fisher Scientific | n/a |
| Clipping station | Sub-angstrom | CSA-01 |
| Compound 2 | n/a | n/a |
| Cryo-FIB specific autogrid rims | Thermo Fisher Scientific | 1205101 |
| E64 | Sigma | E3132 |
| Emitech K100X glow discharge unit | Quorum | n/a |
| Gibco RPMI 1640 media | Thermo Fisher Scientific | 12633012 |
| Giemsa Stain | VWR International | 350864X |
| Glass slides | Thermo Fisher Scientific | 11562203 |
| Grid boxes | Sub-angstrom | PB |
| Grid boxes | Thermo Fisher Scientific | n/a |
| Grid boxes | Agar Scientific | AGG3727 |
| Home-made manual plunge freezing rig | n/a | n/a |
| Human blood | n/a | n/a |
| JEOL 4700F Z JSM with a Leica VCT500 stage cooling system | JEOL | n/a |
| Leica EM ACE600 with a VCT500 cryostage | Leica | n/a |
| Leica EM ACE900 | Leica | n/a |
| Linkam cryo-stage for light microscope | Linkam | Model No. CMS196 |
| Methanol | Sigma | 179957 |
| Nikon Eclipse E200 light microscope | Nikon | n/a |
| Percoll | VWR International | 17-0891-01 |
| Quantifoil copper 200 mesh 2/4 holey carbon EM Finder grids | Quantifoil | N1-C17nCuH2-01 |
| Quantifoil copper 200 mesh 2/4 holey carbon EM grids | Quantifoil | N1-C17nCu20-01 |
| Quorum PP3010 prep-chamber | Quorum | n/a |
| Scios dual beam equipped with a Quorum PP3010 transfer stage | FEI | n/a |
| Staedtler Lumocolor fine black permanent marker pen | Viking Direct | ND538522 |
| TFS Titan Krios 300 kV TEM | Thermo Fisher Scientific | n/a |
| Whatmann grade 1 filter paper | Sigma | WHA1001150 |
| Zeiss Axio Scope A1 light microscope | Zeiss | n/a |

Comments/Description

Direct quote from Thermo

Synthesised by Dr Simon A. Osborne, LifeArc

Formulation used for culturing is custom made (REF 041-91762 A) and includes Albumax, glutamine, HEPES and hypoxanthine supplements

For clipped grids

For clipped grids - direct quote from Thermo Fisher Scientific

With an insulated ethane pot (high-density foam) and liquid nitrogen bath (polystyrene) on a bench top in a containment facility.

UK National Blood and Transplant service

FIB-SEM

sputter coater

e-beam rotary coater. In a humidity controlled room.

Cassettes for clipped and un-clipped grids. In a humidity controlled room.

with Linkam cryo-stage in a humidity controlled room.

Solution for percoll cushion is 35 ml 10x PBS, 150 ml RPMI 1640 media and 315 ml Percoll

100 pack

100 pack

sputter coater

FIB-SEM

TEM equipped with a K2 or K3 camera.

with Linkam cryo-stage in a humidity controlled room.

24/02/2021

Dear Vidhya,

Many thanks to you and the three reviewers for their feedback on our work (JoVE62350). We have been through the comments and implemented many of the changes that the reviewers suggested, producing, in our opinion, a much-improved version of the manuscript.

Please see below a point-by-point response (in blue text) to each comment, including the position in the text where the change has been made.

We have uploaded the new version of the text, along with the revised figures/tables and updated materials table to your editorial manager and we look forward to your response.

Kind Regards,

Claudine Bisson

Editorial comments:

Changes to be made by the Author(s):

1. Please take this opportunity to thoroughly proofread the manuscript to ensure that there are no spelling or grammar issues. E.g. Line 397: (merozoite) instead of "(merozoite0", etc.

The manuscript has been thoroughly checked for typographical errors.

2. Line 141: On what surface are they fixed? Glass slides? Grids?

We have added "on a glass slide" to the text (Line 151).

3. Line 181-182: Please specify the coat thickness for both methods to avoid confusion.

The coat thickness for sputter coating is variable.

4. Lines 197, 210: Please check the values for the ion beam current. Possibly, 1.5 pA is a typo.

This is correct, surveying the sample with the ion beam is done at very low current (1.5 pA) to avoid damaging it during the setup. A higher current (300 pA) is then used for the first milling step.

5. Line 230: Please add details about how this is checked? What are the precautions to be taken etc.

We can provide an additional document with this information, which we were required to check before taking plunge-frozen grids of schizonts to our national facility. I have added a NOTE to provide an overview what we did after protocol step 1.4 – please let me know if this is sufficient.

6. Please do not include manufacturer's details in the protocol. Mention those in the Table of Materials. E.g.: Line 142: VWR Int., Line 146: Sigma etc.

All instances have been removed.

7. Upto 3 pages of protocol can be highlighted and filmed. As the text highlighted is well within this limit, please consider highlighting any additional steps which could add more detail and clarity. Also include a single line spacing between successive protocol steps.

We would have to go to multiple filming sites to film further steps, we can discuss expanding the section filmed at a later date.

8. Avoid use of personal pronouns in the protocol. E.g. "we", "our" etc.

All instances have been removed.

9. Please do not use "&" in the references. Also do not abbreviate the journal names.

All references have now been formatted correctly.

10. Please separate the figure/table legends and add them in a separate section after the representative results. Also, do not embed figures/tables in the manuscript, but upload them separately in the specified formats.

In the revised version we have moved the figure and table legends to a separate section, as requested and I have uploaded high-res images as separate files.

11. Please sort the Materials Table alphabetically by the name of the material.

This has been corrected.

Reviewers' comments:

Reviewer #1:

Manuscript Summary:

The manuscript by Bisson et al. describes the preparation of cryo-lamellae for cryo-electron tomography from *Plasmodium falciparum* infected erythrocytes by focused ion beam. This Cryo-FIB milling has recently received a lot of scientific interest because of the highest level of preservation and the possibility to study cellular processes at molecular resolution. The authors present their workflow for preparation and imaging of lamellae human erythrocytes, a cell type for which to my knowledge this method has not been adapted before. At the same time, they include the relevant literature references to previous studies with different cells and organisms and to ongoing efforts in method development.

While there are several protocol papers published describing comparable workflows for other specimens, only sparse video material is available for this method. Thus, I really like the idea of a video description of this workflow, which will together with the manuscript give a good overview of the steps involved. The adaptations for human erythrocytes described in this workflow will be interesting to cryo-FIB users in general but also for optimization of their own samples.

However, I feel that parts of this manuscript should be presented clearer and should contain more detail in order to avoid confusion especially to novice users. The following points hopefully help to further improve the manuscript:

We thank the reviewer for their constructive feedback and have implemented most of the changes that they suggested, which have improved the protocol substantially. Please see details below.

Major Concerns:

The authors should carefully review their usage of method names throughout the whole manuscript. They sometimes interchangeably use 'FIB-SEM', 'cryoFIB-SEM', 'cryoFIB' technology. The method cryoFIB-SEM also exists and rather describes serial cross-section imaging by FIB-SEM with unstained frozen samples. To avoid confusion, especially to new readers outside the field, please be precise when you are talking about cryo-FIB milling (or cryo-FIB/SEM lamella preparation).

We have amended the usage throughout the text to always use the cryoFIB-SEM terminology when talking about the microscope and FIB-milling when talking about the technique, specifically mentioning plunge-frozen or vitreous samples, where necessary. We have also added a description of the cryo volume imaging approach described by the reviewer, with references (lines 103-105).

Please also review the use of the correct plural form of lamella, which is lamellae. I found numerous examples throughout the text where the plural seemed appropriate. (e.g. line 41, 129, 214, 230, 327, 379, 458). This list is likely not complete, please check.

We have been through the manuscript and checked/corrected the pluralisation of the word lamella, including in the title.

Line 58: '...is an essential step in the reconstruction of high-resolution tomograms...'. Please do not use reconstruction here because this should not be confused with actual tomogram reconstruction (Maybe rather generation or something entirely different).

We have changed this to "...essential step for downstream techniques, including cellular cryoEM, cryoET and sub-tomogram averaging ..." (lines 59-61)

Line 104-105: Limited thickness for cryo-sections. Please cite where this number comes from, also does it refer to the methods limitation or the access to higher resolution information.

We have altered the text to explain that compression artifacts increase with the thickness of the cryo-sections. We've also added a reference for the optimal thickness and now give a range of 40-100 nm. (line 113)

Line 116: 'surface area ($>100^2 \mu\text{m}$). Should probably say $> 100 \mu\text{m}^2$? But how is this number justified? In Fig 6B you show an example with only $30 \mu\text{m}^2$. Does this mean you can't do tomography here? At some point it will of course become too small to fit record and focus area, especially when tilting and the throughput will suffer a lot, but this number seems arbitrary.

We agree, the lower limit is dictated by the surface area required to fit the acquisition and focus areas, therefore this also depends on the magnification. We have deleted this value and explain minimum surface area in later sections (line 127 and 469).

Line 171: You mention the meniscus of ice here and refer to Figure 2, however Figure 2 does not highlight the meniscus and it is not mentioned in the Figure legend.

Meniscus is the wrong term here, the best grid squares should be one cell thick at their centre, so we have changed the text to reflect this (lines 179-185).

Line 175: Cryo-FIB milling: This part is missing information about how to clip the grids into the autogrids, cell side should be facing down during clipping and then up when loading in the cryo-FIB shuttle. This is crucial, because if this is not done correctly, lamella making is not possible.

Yes, this is a very important point that we have now added text to point this out (line 194).

Line 185/186 & 197/198 & 352-358: Please state both voltage and currents used for these steps.

The voltage of the ion beam is 30 kV at all currents (see Table 1 for milling scheme). We have now added this to the text (line 216).

Line 214 - 222: In one paragraph you mention thickness of 0.3 μm in the other thinness of 100-300 nm. I find that misleading, aren't the thicker ones are the same thickness? Does this mean some lamellae have not been polished? It would help to know how many lamellae you make on a single grid. Explain why you start polishing from the front and then move to the back and how long do you take for final polishing (do you limit yourself to approx. 1 h to avoid contamination?)

Yes, we can see why this might be confusing, so we have edited the text in this part of the protocol (2.8-2.13) (lines 226-253) to provide much more detail. We have added a panel to Figure 5 to explain the polishing route and expanded on the other points that the reviewer mentions, in more detail in the representative results (lines 422-445).

Line 234: It is clear to me that the lamella needs to be perpendicular to the tilt axis and why, but I'm not sure I understand the term 'the length of the lamella is aligned to the direction of rotation'.

Yes, trying to labour the point here didn't help with the explanation – this text has been removed.

Similarly, in line 308-09, 'rotation axis' and explanation that follows should be clearer. Tilt axis would be better here (see also line 382 and 545).

We have changed the text to consistently use the correct term – tilt-axis.

Line 240: The pretilt depends on the loading orientation/ direction into the cassette, depending to which side the cutout of autogrid is facing. If loaded 180° rotated, it should be -10°. It would be helpful to mention this somewhere. It might be good to mention how the authors determine the pretilt.

We have added a sentence to the protocol as a NOTE to explain this (after step 3.3).

Line 250 & 254: Use the correct names: MotionCor2, etomo, IMOD

These have now been edited.

Line 457: '(expect 50 %)' Is this value determined anywhere here (if so from how many lamellae/ grids), how reliably is this value or is it rather empirically determined? Also, later in the text you mention micro-expansion gaps which have been shown to reduce overall breakage. Is this value with micro-expansion gaps and if not, would it be helpful to mention that this may reduce the number here in the text.

The 50 % figure is just through our personal experience, some grids will be better than others. We have edited this part of the text to explain this better (lines 550-558).

We have not tried the micro-expansion gaps ourselves, so can't really comment on this, but we wanted to include this paper as it is a new adaptation of the technique and may be helpful in certain circumstances.

Figure 4 and Figure 7: Mark OP and CU in a consistent way. For OP you once use an arrow, in the next panel only writing and then you mark the border. Please find a consistent way that highlights the platinum layer best (maybe make a border for all images). Same for goes for curtaining, use a either an arrow or outline, but not three different ways of highlighting.

OP is now consistently labelled in yellow with a dashed line indicating the extent of the organoplatinum coat (Figure 3 and 6). CU is coloured blue with a bracket showing the region of curtaining, this is now limited only to figure 6 as this is the relevant part of the text.

Line 561 & 602: The carbon layer in both images (Figure 4 B and Figure 7 B) is hard for me to see here from these images. How do you know where it starts? Is this the only the carbon foil on the grids or have they been coated with an additional layer of carbon?

The carbon layer shown in these images is a strip of 2/4 holey carbon film on the EM grid that runs through the lamella. Cells in front of this layer (closer to the ion beam) are on top of the carbon and behind this layer (further away from the ion beam) are below the carbon. With this grid type you usually get a strip of carbon through the lamella, but its position varies depending on the thickness of the cells at the milling position. We have improved the labelling in Figure 3 and 6, but granted it can still be challenging to see. The new figure 5C, showing the loss of contrast during polishing, shows the carbon layer better as a dark black stripe across the middle of the lamella, hopefully this makes it clearer.

Line 618: 'and labelled the same as in part,' reference missing here.

This should be part D, we have edited the text.

Minor Concerns:

Line 35: Please be consistent throughout the whole text with the usage of 'cryo-' or 'cryo '.

For example: In line 35 you use 'cryo electron tomography'. In line 43 'cryo-electron tomography'.

Cryo- is now hyphenated in all text apart from where a defined term e.g cryoFIB-SEM or cryoEM is used.

Line 79: 'bombarded': colloquial, maybe find a more suitable word.

We have changed this to ablated.

Line 153: Does the concentration of cells vary between different preparations and would it be helpful to give a cell concentration here to have a comparable value?

We have given a 50 % haematocrit value (protocol step 1.3), which is the closest approximation of cell concentration you can give for this type of sample. You aim for all the cells to be mature schizonts at the same stage of growth, in reality, the homogeneity of the prep varies each time you purify the schizonts depending on how closely they are synchronised. 50 % haematocrit is rather a thick cell solution, which works well for this sample, other samples will be different.

Line 156: Is it helpful to be more specific about the glow discharging? (model used, from carbon side or both sides, etc.)

We have added this information (protocol step 1.4)

Line 197: Nothing is said here about the width of the lamella and the size of the milling patterns.

Line 204/205: With the height of the milling pattern, do you mean the z size or depth? Since this is related to the milling time, maybe rather the milling duration?

We comment on the width of lamellae in the representative results section (lines 422-432)) but we have also added a note after protocol step 2.6 to provide this information at an appropriate place in the method (line 222). There is no set height for the patterns, it all depends on the thickness of the sample. We usually start around 6 um high for the first milling step, but adjust this on the fly. For subsequent milling steps, the patterns only need to cover the un-milled material. We have included this information in the NOTE after protocol step 2.6 and the text in step 2.8.

Line 227: (5 mA, 8 secs) I would assume this varies between instruments? What is the expected thickness of the Pt layer here in order to be helpful for ET?

Yes, it is very variable even with a set current and timing, so should only be done if you can trust your sputter coater. We have tried different things with this and now choose not to sputter coat routinely, hence why we added this as a NOTE rather than a protocol step. The lamella used in Figure 8 (now Figure 7) was lightly sputter coated after milling and the detail in the tomogram suffered as a result. We have edited the text to explain this (NOTE after protocol step 2.13).

Line 230: What's the benefit of cryo-fluorescence microscopy screening here? This sample doesn't have fluorescence markers? Or is this more meant as a general note? To my knowledge there are only few labs doing this successfully and studies published so far use transformation of fluorescent signals from z-stacks acquired before milling. So doing this is far from standard in my opinion.

We did not use CLEM in this study, so this is meant as a general note. We agree, obtaining z-stack information is far from standard, but correlating X/Y positions to target milling is more straightforward and has been done with a relatively un-complex setup with other samples in our group and by others. It all depends on the strength and distribution of the signal. Screening for fluorescence inside lamellae is more challenging as the lamellae are very thin, so it all depends on the signal strength. It is possible, so we have changed the text to reflect this (line 261) and added an additional NOTE after protocol step 1.5 (line 187).

Line 257: 'outputting unbinned, 2x, 4x, 8x binned tomograms.' Obviously, this very much depends on the downstream application. For segmentation and viewing, you may not want to generate a lot of unbinned tomograms.

Yes, we agree and have changed the text accordingly.

Line 283 & 292: should probably mean 'back side blotting'

We don't like the term back-side blotting but have changed the text to "blotting the grid from the back" in both cases.

Line 296: Is TEM screening with grid maps really useful for this sample, if you have a continuous layer of cells? I would have thought you will mainly get black images even on good grids?

For this sample, we couldn't screen by TEM, but for other samples it would be possible and recommended as you'd have cleaner transfer steps and more information about the ice gradients across the grid. We have changed the text to explain this (lines 340-344).

Line 317: It would be helpful to know that on which side the cutout is when loading determines the pretilt.

We have added information to explain this in NOTE after protocol step 3.3 and a section of text in the "Collecting and processing tilt-series data" section (461-467).

Line 332: 'which sticks to cold surfaces' maybe 'condenses on' is less colloquial.

This has been edited.

Line 375: 'they will just be shorter than usual' maybe add that this results in lower cryo-ET throughput.

Yes, it would, there will be fewer available areas to collect data from, however, you can produce more lamellae from a thinner sample in a single session – so it could work out, depending on the sample. We have explained this in more detail (lines 429-432)

Line 397: typo '(merozoite0.'

This has been corrected.

Line 438: remove 'very'

We have edited this sentence to remove the words “very precious” all together.

Line 444: '(gold is more fragile, copper is more robust, but toxic to some cell types)' Does the metal of the grid really make such a big difference? In terms of softness, gold and copper are almost equally soft (Mohs scale). Also, gold foil is considered more stable. I assume only the grid mesh is meant by gold here, however the statement could be confusing.

Fair point, we really just wanted to point out that you would normally use gold grids for cells because copper can be toxic – it depends on the cell. You can't use gold foil because you can't mill the gold at these low ion beam currents, so it has to be carbon film. We have changed the text to reflect this (lines 536-542).

Line 503: '*polishing should be performed in parallel, where milling areas are active at the same time.' Would be good to give a reason for this, if there is any.

This evenly heats the lamella from both sides as it reaches its final thickness, reducing the risk of the lamella bending or bowing. We have added text to explain this in the legend for Table 1.

Line 527: Figure 2. Scale bar in (B) not shown. Because (B) mentions a 300 mesh grid it would be good to write in (C) that this is a 200 mesh grid.

We have amended the figure legend and added additional annotation to part C to describe the varying ice thickness across the grid square.

Figure 5 F: The lamella edge could be highlighted with an arrow.

A white arrow has been added (now Figure 4F).

Reviewer #2:

Manuscript Summary:

In their manuscript entitled 'Preparing lamella from vitreous biological samples using a dual beam scanning electron microscope for cryo-electron tomography' Bisson et al. describe a protocol for site-specific thinning of vitrified specimens for subsequent analyses by cryo-electron tomography. The title and abstract are in accordance with the paper content. The introduction properly sets the stage, however, the authors should mention the most recent developments in the field, e.g. the automated cryoFIB protocols implemented by the Pilhofer and De Marco labs (eLife and JSB papers published last year). Also, cryoET of in vitro specimens and viruses should be mentioned in line 67 as this is where cryoET earned the reputation of a technique capable of producing high resolution information (e.g. Briggs group work on HIV). Finally, the authors should emphasize that cryoET is helpful to address not only biological problems that require high-resolution information obtained by subtomogram averaging but also complex cell biological phenomena where broader cellular context is required (e.g. bacterial cell division investigated by the Jensen and Lowe groups).

We thank the reviewer for their feedback and the additional references, which now been incorporated into the relevant sections in the introduction or discussion. We hope this provides the reviewer with the extra context that they were looking for. Please see our responses to their other comments below.

Major Concerns:

Currently there are several detailed papers describing protocols for cryoFIB of biological samples (e.g. from the Plitzko and Villa groups) that enable other researchers highly efficient implementation of this technique in their labs. With this respect the submitted manuscript is neither novel (which is not required by JOVE) nor efficient, as I will discuss further. In their discussion, the authors put emphasis on sample preparation optimisation but the manuscript itself is very scarce when it comes to comprehensive sample optimisation that would yield reproducible results.

The reviewer is fair to point out that our method is not novel and there are other publications that describe much more sophisticated approaches to FIB-SEM. We reference these groups work in our manuscript. We did not intend to write a proof-of-principle method, instead we wanted to describe our journey through sample optimisation of malarial schizonts, which have not been prepared in this way before and relay what we have learnt to others who might be embarking on FIB-SEM with other novel samples. We do this using basic tools found in most EM labs and in partnership with our national facility as well as local collaborators. The protocol presented here is therefore an accessible guide through the critical steps of optimising samples for FIB-SEM, which we hope will inform others who may be new to this technique. It may not be the most efficient workflow, but we do achieve reproducible grids, therefore this shows what can be done with more limited resources, making the basic technique more accessible.

Given that schizonts are not adherent cells grown on EM grids but applied as a solution directly before plunge freezing, the authors should estimate what's the optimal schizonts concentration (in cells/ml) that results in a uniform layer suitable for cryoFIB.

50 % haematocrit is % v/v red blood cells (in this case schizonts) to growth media, which is the standard way of quoting concentrations for this sample. This makes a fairly dense cell suspension and is the most appropriate way to describe the cell concentration in this case. For different cell types, the cell density would have to be optimised in each case given how the cells interact with the grid, the grid type, the blotting conditions, the cells themselves etc, so we don't think providing cell/ml concentration is actually that helpful to others.

Given that a vast majority of the labs use automated systems for plunge freezing (e.g. Vitrobot or Leica systems) I am surprised that the authors did not include even a brief discussion on what would be initial plunge freezing parameters there (humidity, temp, double vs. one sided blotting etc.).

We used a bench top manual freezing rig, which was located inside a containment 3 facility and fully describe the method. The nature of a manual rig is that it is exposed to changes in the local environment - temp, humidity and air-flow all fluctuate - but despite this, we were able to make reproducible grids.

We do briefly discuss the setup for an automated plunge freezer, but the specific settings would depend on the cell-type and the actual plunge freezer used – therefore this is all part of the optimisation process. For schizonts, we would probably start with room temperature and high humidity (~70%), which we have now added to the text (lines 334-338). We also discuss this across lines 536-542 in the discussion.

Finally, I am concerned about employing cryoLM solely for sample screening, unless additional information for cryoCLEM purposes is obtained during the process. Performing cryoLM is always associated with additional cryo-transfers and sample exposure to the environment, which inevitably leads to ice contamination etc. I believe that once optimal and reproducible sample prep conditions are found there is no need for cryoLM, particularly if it is to be performed on bare grids (paragraph starting at line 169).

In our hands we did not experience excessive surface contamination when screening by light microscopy, but it is true that screening by TEM would be cleaner. We couldn't do this as our grids were too thick (See additional TEM overview in Figure 6A). Once reproducible blotting and plunge freezing conditions had been optimised for this sample, we didn't need to screen all of the grids by light microscopy and often milled grids without screening them first. We have added some text to explain this (lines 340-349).

I am also concerned with the quality of the data presented in Figure 8 - membrane appearance is akin to that of a devitrified sample. The authors should include more other examples to convince readers about the efficacy and robustness of the protocol.

There was no clear evidence of devitrification in this lamella or the grid in general, although we can't rule out a minor effect. If the sample had suffered radiation damage during the tilt-series acquisition we would have seen this in the state of the rhoptry contents, which are the first thing to melt in these samples if they experience excessive dose. We think that the lack of clarity in the membranes is due to the sputter coating applied to the grid after milling (now shown in Figure 7E), which has made the contrast lower and therefore effected the reconstruction slightly. We have added some zoomed in views of some of the membranes from the sample showing that the lipid bilayer is visible in the tomogram, indicating it is of sufficient quality for analysis. In addition, we have added a second tomogram, plus annotations to Figure 8, showing the apical end in a mature merozoite. This lamella was not sputter coated after milling and we hope the improved contrast is clear.

Minor Concerns:

Line 68 - would add 'cryo' before focused ion beam (FIB)-milling to emphasize difference from materials sciences

We do say that this is at cryogenic temperatures later in the sentence. Based on feedback from all the reviewers, we have been through the text and made the terminology more consistent.

Line 78: is focused ion bean, should be beam

Good spot – thanks for that.

Line 79: re-phrase, 'ions generated by a gallium source'

Yes, this reads more cleanly, we have made this correction.

Line 85: 'transfer' replace with 'sample transfer'

Yes, this should be sample transfer, we have made this correction.

Line 113-114 - it is possible to prepare on grid lamella of high pressure frozen samples without cryo lift out although laborious (Medalia's group Nature Methods 2015 paper)

Yes, that's the reference to adapted sample carriers for high-pressure frozen samples (ref. 28 Harapin et al, 2015) which is used here.

Line 153 - 2.4 x g ???

This is an error, it should be 240 x g, we have corrected this.

Line 172 - why one cell thick? Two or three cell thick layer should still be capable of vitrification and produce longer lamellae.

A lamella is milled through the sample at a shallow angle, so captures multiple cells both above and below the carbon layer as a strip across the centre of the grid square. Ensuring that the grid square is one cell thick in the middle, means that the ion beam should break through above and below the lamella avoiding the thicker ice next to grid bars. If the ion beam does not break through you produce a wedge, rather than a free lamella, which is not as useful for tomography and in our experience, can have crystalline ice in its thicker parts. From a practical point of view, it is more time efficient to mill somewhere you know is on the thinner side as you will make quicker progress with the initial cut, rather than milling somewhere thicker and waiting for ages during the initial cut to see if the ion beam has broken through or not.

Line 397 -) is missing

This has been corrected.

Figure 2B - scale bar missing. Also, using a 300 mesh grid for subsequent cryoET work is not an ideal choice

Agreed, that is why we used 200 mesh finder grids in our study. Figure 2B shows a trial with 5/2 square holey carbon (which happened to be on a 300 mesh support). The hole size matches the cell size quite well, so we wondered if this might produce a nice monolayer of schizonts. In fact, the samples were usually far too thin and produced unstable lamellae. The scale bars for parts A and B are the same.

Figure 2C - please highlight the relevant cells/structures with arrows/arrowheads

We have amended this figure to point out the structures mentioned.

Figure 5B - can't really see what the arrows point to

The purpose of this image is to demonstrate the change in contrast when you increase the energy of the SEM to 30 kV, enabling the operator to screen ice thickness and in this case, the position of the letters and number on the finder grid. We have added an inset to the figure (now Figure 4B) to make this clearer.

Figure 8 - the specimen appears to be devitrified

As discussed earlier in our response, we think the sputter coat has made the membranes appear less clear in the tomogram.

Line 390-391 - authors should discuss the pixel size issue not only in the context of desired final resolution but also the field of view

Agreed, we have added text to explain this in more detail (lines 468-470).

Reviewer #3:

Manuscript Summary:

This paper provides a good and useful description of the method of making cryo-lamellae from plunge frozen grids of cells. While the authors use *Plasmodium falciparum*-infected red blood cells (RBC) in this study as a model system to outline their protocol, they mention that this can be easily adapted to other biological systems, which is useful and interesting.

The primary techniques used in this study encompass preparation of schizonts (malaria infected RBC's), optimizing grids and conditions for manual plunge freezing, screening ice quality by light microscopy, optimizing organoplatinum coating thickness and FIB milling steps to obtain the best lamellae and subsequent cryo-electron tomography. While the paper largely focuses on the protocol for obtaining well milled cryo-lamellae, some insights into the observed structure of the merozoite within the RBC's to what is already known has been proposed.

The protocol outlined here aims to serve as a general guide for obtaining well milled cryo lamellae. However with this in mind, my main criticism is that some aspects have information missing and are less adequately explained. These can be easily rectified and further strengthened by providing more detailed explanation and figures in the paper.

We thank the reviewer for their comments, some of which have already been addressed by our responses to the other two reviews, any additional changes in direct response to reviewer 3's comments are outlined below.

Major Concerns:

1) Page 4, line 171

The importance of ice quality while screening grids with a light microscope is mentioned specifically with reference to the ice meniscus around each square in the grid as shown in Figure 2. But looking at the figure 2, it is not completely clear where exactly this meniscus is. It would be good to clearly label the meniscus or annotate it in some way. Also helpful would be a higher magnified figure comparing how the meniscus looks (rather than ice thickness in general) in a less ideal state (more thick or more thin).

We have changed this part of the protocol as we weren't satisfied that looking at the meniscus was in fact a good way of judging the ice thickness. It is more important that the ice at the centre of the grid square is one cell thick (or down to the carbon), this ensures that you can mill a lamella starting at the centre of the grid square without hitting the very thick ice around the edges of the grid square next to the grid bars (see edited text in protocol section 1.5 and line 345 in representative results). Additionally, we have annotated Figure 2C to indicate good milling positions and where the ice is too thick around the edge.

2) Page 4, line 189

The authors mention the thickness of the organoplatinum coating on the sample being crucial and needing to be $> 2\mu\text{m}$ to preserve the integrity of the lamellae. Considering this is a method that would allow others to replicate and follow, its important to provide as many details of the application conditions including temperature of the GIS, sputtering time and the distance from the grid during sputtering. A table collating all the data relating to application conditions carried out by the authors on their system in relation to the above parameters will provide greater clarity and insights into what worked and didn't work.

We have added temperature and timing details as a guide (protocol step 2.4 and NOTE), but the settings will differ by instrument, so we have provided additional detail about this in the relevant representative results section (lines 379-403). As a user at a

national facility you may not be able to do much about the settings for the GIS, but you can ensure that you pick a milling spot where the coating and the sample looks good, which we have also now explained in more detail.

3) Page 5, line 215-218

The text refers to planning a polishing route of the milled lamellae from the closest one to the ion source to the farthest away. It would be useful to add more details in the text as to why this is seemingly quite important as pointed by the authors and/or what is the result of not following that methodology.

We have now explained why this is important in protocol step 2.11 and lines 442-445, plus we've added a schematic (Figure 5D).

4) Page 6, line 279

The paper clearly points to grid optimization prior to milling as being crucial and a major focus of this paper. However, not enough details have been furnished for plunge freezing optimization with other grids, although it is mentioned that they were trialed. For example, Figure 2 shows use of only one other type of grid other than the Quantifoil 2/4 200 mesh ones that suit best for the cells used here. A list of the other grids trialed alongside their freezing conditions tested and why they were not compatible will provide thorough information. Further, comparable figures of these various frozen grid types will render more useful information and clarity.

Unfortunately, we don't have a set of high enough resolution images showing all of the grid types that we're trialed, but we have added text to the representative results to describe this optimisation step (lines 319-329).

5) Page 9, line 385

A possible aspect of transfer damage may also include sample being partially devitrified. Showing a figure for comparison if possible of an intact lamella and a lamella partially devitrified after transfer will be useful for using this protocol as a general guide of "what not to obtain".

We have added a panel B to Figure 6 showing a lamella containing crystalline ice, indicating either poor vitrification or devitrification during one of the transfer steps. In this case, it's probably the former as the milled region entered thicker ice around the edge of the grid square, such that the FIB could not break through the back edge of the lamella, which generated a wedge. This lamella didn't provide any useful tomography positions as it was also severely cracked, had large particles of surface contamination and shelves of un-milled material towards the back edge, which obscured the view of the sample at high-tilt. Text to describe this has been added to the figure legend and text (line 454).

6) Page 10, line 420-424

The authors refer to the striking difference in morphology of their observed merozoite after RBC invasion as seen by cryo tomography as compared to the mature merozoite prior to infection. However, this feature is not entirely novel and has been observed previously by Hanssen E et al (Cellular Microbiology, 2013) showing fusion of rhoptries in invading/post invasion merozoites.

The reviewer is right to point out that our observation is not entirely novel and that similar observations have been reported previously using fixed and stained parasite material in resin sections. Hanssen et al report the morphology of fused rhoptries prior to invasion, but many outstanding questions are posed in their paper concerning how the fused rhoptries maintain their shape and what happens to them after invasion. Where our observation differs is that the merozoite has fully invaded and we observe details of a complicated membrane structure surrounding the fused rhoptries, plus a lack of IMC in the merozoite, suggesting that these membranes may be what's left over of the IMC after invasion. We also see a closely juxtaposed double membrane surrounding the invaded parasite and many multi-layered vesicles within its cytoplasm. These features are new and have not been shown in unfixed and unstained cryo samples before, representing, in our view, novel details from a step in parasite invasion, prior to the formation of a ring-stage parasite. As such we think this is interesting to the malaria field. We have added some more analysis to compare our observations to those from Hanssen et al and referenced this and other papers to support our conclusions. We think that these additions have strengthened this section of the paper and would like to thank the reviewer for their feedback on this.

7) Page 11, line 442

Although the authors mention that the focus of this work is optimization of grids for various cell types, they have only presented optimized trials for one cell type - malaria infected red blood cells.

The focus of our work was not to optimise grids for all cell types, the project focussed solely on *P. falciparum* schizonts. However, any cell suspension could be plunge-frozen and milled using a slightly modified version of our protocol, which is what the section of the discussion starting line 536 explores. The critical steps in the approach would be no different, but the specifics at each stage would need to be optimised for the particular cell type and instruments used. We have modified the text at the start of this section to emphasise this point.

8) Figure 5

The authors mention that polishing is stopped when loss of contrast is observed. However looking at the image, it is not abundantly clear as to what is the loss of contrast they refer to. As this step is unarguably important to obtain thin electron-transparent intact lamella, an image with a lamella prior to achieving loss of contrast and stopping the polishing will provide greater clarity and understanding on the exact timing of this event.

We have added a new panel C to what is now Figure 5 to show this. An explanation is given in the figure legend.

9) Figure 8

Although the position of the sputter coat applied to the lamella after milling is indicated by the black arrow in Figure 5E, this is not entirely clear. Annotating it in both Figures 8D and 8E will be more useful to follow.

The two coatings that the reviewer is talking about here are different things. The first is the organoplatinum coat applied via the GIS needle before milling, seen as the bright white stripe in Figure 5E (now Figure 4E) and dark black layers, labelled OP, in Figure 7C and D (now Figure 6C and D). The second is a sputter coat of platinum that can be optionally applied to the grid after milling, which helps disperse charging in the TEM, indicated by the black arrow in Figure 8E (now Figure 7E). We have changed the annotation in Figures 4 and 6, to make the organoplatinum coat clearer and changed the figure legend in Figure 7 to explain that this is a different coating.

10) All images including light microscopy and cryo SEM/TEM images do not show the size of the scale bars. This needs to be clearly displayed in all images.

The scale bar sizes are indicated in the figure legends.

Minor Concerns:

1) Page 4, line 197

Information relating to when the ion current 1.5 pA is used is not entirely clear and confusing at times. While Table 1 outline currents used for the step-wise milling steps (300pA to 30pA for the polishing), it doesn't include the use of 1.5 pA. Clarification is needed if this is only used for visualization and imaging and nothing to do with milling or otherwise.

We have added text to the protocol (step 2.6) to explain this more clearly and to the legend for Table 1.

2) Page 4, line 202

More information on the milling pattern parameters, such as if the rectangle patterns are milled one after the other and from which end - top to bottom or vice versa will enable greater clarity while trying to replicate the protocol. The authors have also used SEM imaging intermittently during the milling to check if it looks ok. Information relating to what voltage/current and how often this was carried out to avoid burning the sample will prove useful.

On the Scios cryoFIBSEM milling is carried out in parallel (where both patterns are milled concurrently) using the default "Rectangle" milling pattern. The lower pattern is rotated 180° so milling is performed toward the faces of the lamella. On the JEOL cryoFIBSEM milling is carried out sequentially, the top pattern is milled first (same beam path) and then the bottom pattern is milled afterwards, except for the final polishing step, where parallel milling is used. We have added an extra NOTE after protocol step 2.6 (line 226) to explain this.

For the SEM imaging voltage/current, see response to next point.

3) Page 5, line 220

More detail regarding how often frequent monitoring by SEM during polishing at 3KV without causing sample radiation was carried out will help further clarifications. Additionally, it would be useful to see some numerical parameters such as speed of image rastering, image resolution and image averaging used.

Imaging parameters for the SEM during the final thinning process, typically are 2 – 3 kV, 13 pA, dwell = 300 n, 3072 x 2048, taking ~ 2 s for a full frame, with no frame or line integration averaging. We have added this information to protocol step 2.12 (line 253). To limit radiation damage, the frequency of SEM imaging is minimized only for necessary monitoring.

4) Page 5, line 238

Provide values of low and medium magnifications used for acquiring the maps by cryo-TEM.

The magnification used for the medium-magnification montages will depend on the size of the lamella, but we have added some details to protocol step 3.2 as guidance.

5) Page 7, line 297-298

Annotate meniscus for further clarification in Figure 2 (see comment 1)

Please see earlier response to comment 1 from reviewer 3.

6) Page 7, line 318

Specify the names of inks tried and used that did not interfere with the milling.

We used Staedtler Lumocolor permanent pens to mark the rim. They seem to work fine, so we have added this to the text (line 368).

7) Page 9, line 383

Actual magnification used to obtain the medium magnification montage maps for each of the lamellae needs to be provided.

See response to point 4 above.

8) Page 10, line 397

In the statement "The example shown here (Figure 8) contains a red blood cell that has recently been invaded by *P. falciparum* parasite (merozoite0", the 0 needs to be replaced with a close bracket.

We have now corrected this error.

9) Figure 1

Adding labels denoting the various structures such as vacuole, merozoites, haemoglobin and hemozoin crystals to the figure will enable further clarity.

We have added a schematic to each image indicating these cellular features. This also helps understand Figure 2C.